

## Journal Pre-proofs

Anticancer potential of novel  $\alpha,\beta$ -unsaturated  $\gamma$ -lactam derivatives targeting the PI3K/AKT signaling pathway

Matteo Brindisi, Luca Frattaruolo, Raffaella Mancuso, Antonio Palumbo Piccionello, Ida Zicarelli, Marco Catto, Orazio Nicolotti, Cosimo D. Altomare, Bartolo Gabriele, Anna Rita Cappello

PII: S0006-2952(21)00272-0  
DOI: <https://doi.org/10.1016/j.bcp.2021.114659>  
Reference: BCP 114659

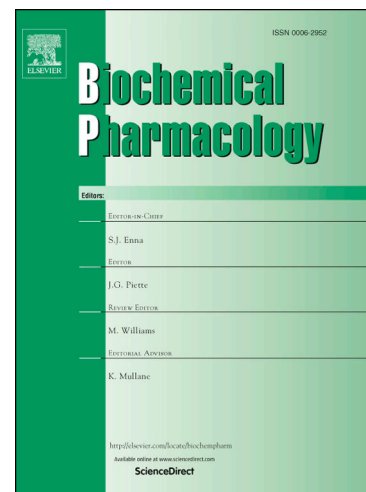
To appear in: *Biochemical Pharmacology*

Received Date: 1 April 2021  
Revised Date: 14 June 2021  
Accepted Date: 15 June 2021

Please cite this article as: M. Brindisi, L. Frattaruolo, R. Mancuso, A. Palumbo Piccionello, I. Zicarelli, M. Catto, O. Nicolotti, C.D. Altomare, B. Gabriele, A. Rita Cappello, Anticancer potential of novel  $\alpha,\beta$ -unsaturated  $\gamma$ -lactam derivatives targeting the PI3K/AKT signaling pathway, *Biochemical Pharmacology* (2021), doi: <https://doi.org/10.1016/j.bcp.2021.114659>

This is a PDF file of an article that has undergone enhancements after acceptance, such as the addition of a cover page and metadata, and formatting for readability, but it is not yet the definitive version of record. This version will undergo additional copyediting, typesetting and review before it is published in its final form, but we are providing this version to give early visibility of the article. Please note that, during the production process, errors may be discovered which could affect the content, and all legal disclaimers that apply to the journal pertain.

© 2021 Published by Elsevier Inc.



## the PI3K/AKT signaling pathway

Matteo Brindisi,<sup>a</sup> Luca Frattaruolo,<sup>a</sup> Raffaella Mancuso,<sup>b</sup> Antonio Palumbo Piccionello,<sup>c</sup> Ida Zicarelli,<sup>b</sup> Marco Catto,<sup>d</sup> Orazio Nicolotti,<sup>d</sup> Cosimo D. Altomare,<sup>d\*</sup> Bartolo Gabriele<sup>b‡</sup> and Anna Rita Cappello,<sup>a\*\*‡</sup>

<sup>a</sup> Department of Pharmacy, Health and Nutritional Sciences, University of Calabria, Via P. Bucci, 87036 Arcavacata di Rende (CS), Italy.

<sup>b</sup> Laboratory of Industrial and Synthetic Organic Chemistry (LISOC), Department of Chemistry and Chemical Technologies, University of Calabria, Via Pietro Bucci 12/C, 87036 Arcavacata di Rende (CS), Italy.

<sup>c</sup> Department of Biological, Chemical and Pharmaceutical Science and Technology-STEBCIF, University of Palermo, Viale delle Scienze Ed.17, Palermo 90128, Italy.

<sup>d</sup> Department of Pharmacy-Pharmaceutical Sciences, University of Bari Aldo Moro, Via E. Orabona, 4, 70126 Bari, Italy.

\* Corresponding authors. Email: annarita.cappello@unical.it (A.R.C.);

cosimodamiano.altomare@uniba.it (C.D.A.).

‡ Joint senior authors.

Six recently synthesized alkyl (*Z*)-2-(2-oxopyrrolidin-3-ylidene)acetates were evaluated for their potential as cytotoxic and anticancer agents. All compounds were tested in the ER $\alpha$  positive MCF-7, triple negative MDA-MB-231, and Her2<sup>+</sup> SKBR-3 breast cancer cell lines. The most lipophilic derivatives, bearing the 4-isopropylphenyl (**2**) or 4-*tert*-butylphenyl (**3**) group at the  $\gamma$ -lactam nitrogen, proved to be cytotoxic against all the cancer cell lines tested (IC<sub>50</sub> values ranging from 18 to 63  $\mu$ M), exerting their greatest activity in SKBR-3 cells, with IC<sub>50</sub> values of 33 and 18  $\mu$ M, respectively. Biological studies showed that the cytotoxic effects of **2** and **3** are accompanied by apoptotic death in breast cancer cells, and both compounds showed no significant toxicity on healthy cells (e.g., MCF-10A) and red blood cells. An in-depth mechanistic study based on molecular biology, immunoblotting analysis and *in silico* docking calculations suggested that  $\alpha,\beta$ -unsaturated  $\gamma$ -lactam derivatives could interfere with the functioning of PI3K and PDK-1, two key enzymes in the PI3K/AKT signaling pathway, whose overactivation is related to the regulation of cell growth and survival in several malignancies.

**Keywords:**  $\alpha,\beta$ -unsaturated lactams;  $\alpha$ -methylene- $\gamma$ -lactams; breast cancer; cytotoxicity; apoptosis; PI3K/AKT signaling pathway.

Cancer remains a major cause of death worldwide, with more than eight million deaths, and among the neoplastic pathologies, breast cancer holds the primacy in women as the tumor with the highest number of diagnosed cases [1]. Early diagnosis and personalized treatments may greatly improve patient survival, preventing any increase in tumor size and in the spread of distant metastases, which drastically worsen the clinical outcome in the event of poor drug responsiveness [2]. In this challenging context, the discovery and development of novel efficient and less toxic drugs for breast cancer treatment continue to represent a goal of major importance [3-5].

In this study, we evaluated the biological potential of the 2-(2-oxopyrrolidin-3-ylidene)acetate moiety (Figure 1) as a prospective less toxic anticancer pharmacophore.  $\alpha$ -Alkylidene  $\gamma$ -lactams, which could serve as Michael acceptors of biological importance, are less common in nature and generally less cytotoxic than the related  $\alpha$ -alkylidene  $\gamma$ -lactones [6]. Some representative natural products incorporating the  $\alpha$ -methylene  $\gamma$ -lactam pharmacophore into their structure include the skin irritant pukeleimide E, isolated from the cyanobacterium *Lyngbya majuscula* [7], theazole alkaloid anatin, a remedy for pain made from the leaves of *Cynometra*, an African plant [8], and the bis-indole derivative violacein of bacterial origin, endowed with anti-infective activity against Gram-positive pathogens [9] (Figure 1). Several  $\alpha$ -methylene  $\gamma$ -lactam-containing synthetic analogs have also been evaluated as cytotoxic [10, 11] and anti-inflammatory [12] agents.

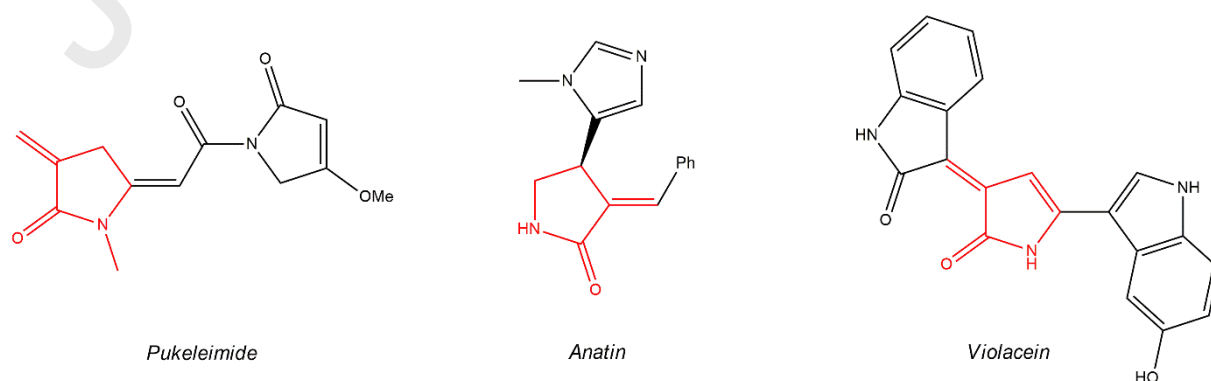


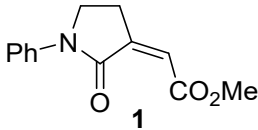
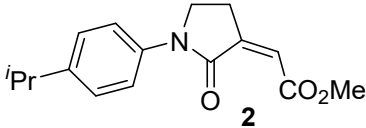
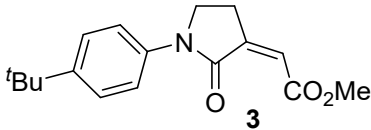
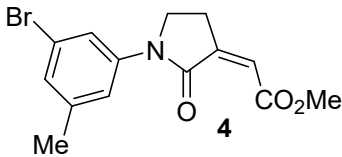
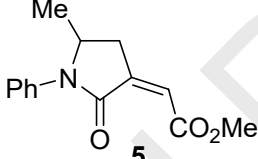
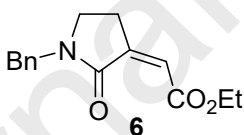
**Figure 1.** Examples of bioactive natural and synthetic products containing  $\alpha$ -methylene- $\gamma$ -lactam moiety (red).

Herein, we report on the evaluation of the cytotoxic and anticancer potential of some  $\alpha$ -methylene- $\gamma$ -lactam derivatives, namely alkyl (*Z*)-2-(2-oxopyrrolidin-3-ylidene)acetates **1-6** (Table 1), very recently synthesized by Gabriele et al. using an efficient and sustainable synthetic approach based on the catalytic carbonylation of readily available homopropargylic amines [13]. The presence of the electron-withdrawing  $-\text{CO}_2\text{R}$  ester group on the exocyclic double bond may increase the reactivity as a Michael acceptor of the  $\alpha$ -methylene- $\gamma$ -lactam moiety toward biological nucleophiles (e.g., thiol group of cysteine residues). Similar compounds bearing the 2-(2-oxopyrrolidin-3-yl)acetate moiety have been studied for their peptidomimetic inhibitory effect [14], and anti-hepatitis B [15], anti-stroke [16], and anti-thrombotic [17] activity; to the best of our knowledge, however, no anticancer activity potential has been reported so far.

This study aims at evaluating the alkyl 2-(2-oxopyrrolidin-3-ylidene)acetate moiety as a privileged chemotype of novel anticancer agents targeted at breast cancer subtypes. To this purpose, six newly synthesized compounds (Table 1), mainly varying in their hydrophobicity (their calculated log P values span a range of 1.7 log units) and bulkiness, were first evaluated for breast cancer cell viability in three different cell models, namely the ER $\alpha$  positive MCF-7, triple negative MDA-MB-231, and Her2<sup>+</sup> SKBR-3 breast cancer cell lines. A subsequent in-depth mechanistic study, carried out with the most active compounds **2** and **3**, allowed us to identify the PI3K/AKT signaling pathway, whose overactivation is closely related to the regulation of cell growth and survival in several malignancies [18], as a target of the  $\alpha,\beta$ -unsaturated  $\gamma$ -lactam derivatives investigated herein.

Journal Pre-proofs

**Table 1.** Structures and lipophilicity of the investigated alkyl (*Z*)-2-(2-oxopyrrolidin-3-ylidene)acetate derivatives.  
Journal Pre-proofs

Compound	Log <i>P</i> <sup>a</sup>
 <b>1</b>	0.915
 <b>2</b>	2.254
 <b>3</b>	2.603
 <b>4</b>	2.277
 <b>5</b>	1.407
 <b>6</b>	1.483

<sup>a</sup> Calculated by ACDLabs software release 10.0 (Advanced Chemistry Development, Inc., Toronto, Canada).

## 2. Materials and methods

### 2.1. Cell cultures

Cell lines used in this study, human breast cancer ER<sup>+</sup> cells (MCF-7), triple negative breast adenocarcinoma cell line (MDA-MB-231), Her2<sup>+</sup> breast cancer cells (SKBR-3), human mammary epithelial cells (MCF-10A) and human endothelial cells (Ea HY926) were purchased

MCF-7 and MDA-MB-231 cells were cultured in DMEM/F12 (Sigma Aldrich, Milan, Italy) supplemented with 10% fetal bovine serum (FBS, Sigma Aldrich, Milan, Italy), 2 mM L-glutamine (Sigma Aldrich, Milan, Italy), and 1% penicillin/streptomycin (Sigma Aldrich, Milan, Italy). SKBR3 cell line was cultured in RPMI-1640 (Sigma Aldrich, Milan, Italy) supplemented with 10% fetal bovine serum (FBS), 2 mM L-glutamine, and 1% penicillin/streptomycin. Ea HY926 cell line was cultured in DMEM high glucose (Sigma Aldrich, Milan, Italy) supplemented with 10% fetal bovine serum (FBS), 2 mM L-glutamine, and 1% penicillin/streptomycin. MCF-10A cells were cultured as previously reported [5]. All cell lines were cultured at 37 °C with 5% CO<sub>2</sub> in a humidified atmosphere.

### 2.2. Cell viability assay

MCF-7, SKBR-3, MDA-MB-231 and MCF-10A cell lines were seeded in 48-well plates with a density of  $2 \times 10^4$  cells/well and cultured overnight in complete medium. Then, cells were treated with different concentrations (100, 75, 50 and 25  $\mu$ M; compounds were solubilized in DMSO) of compounds **1-6**, or co-treated with hEGF (Sigma Aldrich, Milan, Italy) 20 ng/mL for 5 days. DMSO (Sigma Aldrich, Milan, Italy) was used as a vehicle control. At the end of treatment, cell viability was assessed using sulforhodamine B (SRB, Sigma Aldrich, Milan, Italy) assay, as previously described [19]. Non-linear regression analysis GraphPad Prism 8 (GraphPad Inc., San Diego, CA) was used to generate sigmoidal dose-response curves to calculate IC<sub>50</sub> values for each cell line.

### 2.3. Growth curves

Treatments for growth curve experiments of MCF-7, SKBR-3, MDA-MB-231 cell lines were performed in two different ways:

- Cells were treated with **2** or **3** at IC<sub>50</sub> value for 5 days.
- Cells were treated with **2** or **3** at IC<sub>50</sub> value for 1 day and then treatments were replaced by fresh medium left to incubate for a further 4 days.



SRB assay every day for 5 days, starting from day 0.

#### 2.4. Comet Assay

MCF-7, SKBR-3 and MDA-MB-231 cell lines were seeded in 6-well plates with a density of  $3 \times 10^5$  cells/well and cultured overnight in complete medium. Then, cells were treated for 120 h with **2** and **3**. At the end of treatment, cells were trypsinized and diluted with equal amounts of complete medium and subjected to comet assay as previously described [20]. Photographs of slides were taken at  $20\times$  on a fluorescent microscope, further magnifications of cells were obtained using a  $100\times$  objective lens.

#### 2.5. TUNEL assay

MCF-7, SKBR-3 and MDA-MB-231 cell lines were seeded on glass slides in 6-well plates with a density of  $2 \times 10^5$  cells/well and cultured overnight in complete medium. Then, cells were treated for 120 h with **2** and **3**. At the end of treatment, cells were subjected to TUNEL assay (Promega, Milan, Italy) as previously described [4]. Photographs of slides were taken at  $20\times$  on a fluorescent microscope. Apoptotic cells were counted and expressed as % of apoptotic cells, each one vs untreated control.

#### 2.6. Colony formation assay

MCF-7, SKBR-3 and MDA-MB-231 cells in exponential growth period were seeded in 12-well plates (500 cells/well) and grown overnight in complete medium. Then, the assay was divided into two different tasks: Task 1, cells were treated with **2** or **3** at  $IC_{50}$  concentration for 7 days; Task 2, cells after 1 day of treatment with **2** or **3** at  $IC_{50}$  concentration were cultured in fresh medium until day 7. Thereafter, colonies were washed three times with PBS, fixed and stained with Coomassie brilliant blue for 10 min. Subsequently, the excess stain was washed with water. Plates were dried, and photographs were taken by scanning the well plate and are representative of three independent experiments.

#### 2.7. Wound-healing scratch assay

MCF-7, SKBR-3 and MDA-MB-231 cells were seeded into 6-well plates and cultured overnight in complete medium. Then, cells were treated for 24 h with **2** and **3** and cell motility was assessed by wound-healing scratch assay as previously described [5]. Photographs were taken at 4× magnification using phase-contrast microscopy and are representative of three independent experiments. The wound healing rate was quantified from the picture using Adobe Photoshop software and standard deviations were determined by GraphPad-Prism 8 software.

### 2.8. Tube formation assay

Angiogenesis power was assessed by tube formation assay, as previously described [21]. Briefly, Geltrex (Thermo Fisher Scientific, Waltham, MA, USA) was thawed at 4 °C overnight and used to coat a 96-well plate, which was then incubated at room temperature for 30 minutes to solidify. Thereafter, Ea HY926 cells were trypsinized, washed with PBS to remove trypsin and resuspended in conditioned medium obtained from MCF-7, SKBR-3 and MDA-MB-231 cells treated with **2** or **3** at IC<sub>50</sub> value for 1 day. Then, Ea HY926 cells were plated on the Geltrex (4×10<sup>4</sup> cells/well). After incubation for 6-8 h, the newly formed vascular tube networks were photographed. Photographs were taken at 4× magnification using phase-contrast microscopy and are representative of three independent experiments. In a parallel experiment, the viability of Ea HY926 cells treated with conditioned medium obtained from MCF-7, SKBR-3 and MDA-MB-231 was assessed using SRB assay as mentioned above.

### 2.9. Mammosphere formation assay

A single cell suspension of MCF-7, SKBR-3 and MDA-MB-231 were seeded at a density of 5000 cells/well in a mammosphere medium [22] under non-adherent conditions in 6-well plates pre-coated with 2-hydroxyethylmethacrylate (poly-HEMA, Sigma Aldrich, Milan, Italy), and then were exposed to **2** and **3** at their respective IC<sub>50</sub> values and subjected to mammosphere formation assay, as previously described [22]. Vehicle alone (DMSO)-treated cells were processed in parallel as a control. After five days of incubation, 3D-spheres > 50 μm were counted and the percentage of cells that formed spheres was calculated, being referred to as the percentage of mammosphere formation efficiency (MFE).

Immunofluorescence staining was assessed as previously described [23]. Briefly, MCF-7, SKBR-3 and MDA-MB-231 cell lines were seeded upon coverslips inside 6-well plates with a density of  $1 \times 10^5$  cells/well and cultured overnight in complete medium. Then, cells were treated for 24 h with **2** and **3** at their respective  $IC_{50}$  values. Cells were then fixed with ice-cold methanol for 10 minutes at  $-20^\circ\text{C}$ . After fixing, cells were washed three times for 5 minutes with TBS and then incubated for blocking with 5% BSA in TBS for 40 minutes at  $37^\circ\text{C}$ . Then, cells were incubated for 40 minutes at  $37^\circ\text{C}$  in 1:200 anti- $\alpha$ -tubulin monoclonal antibody (Santa-Cruz Biotechnology, CA, USA). After incubation with the primary antibody, cells were washed three times for 5 minutes with TBS to discard excess primary antibody. Then, cells were incubated for 40 minutes at  $37^\circ\text{C}$  in 1:300 anti-mouse IgG-TRITC (Sigma Aldrich, Milan, Italy) and subsequently washed three times for 5 minutes with TBS. To stain the nuclei, cells were incubated with DAPI solutions ( $0.2 \mu\text{g/mL}$ ). Slides were visualized using a  $40\times$  objective on a fluorescent microscope.

### 2.11. Immunoblotting analysis

MCF-7, SKBR-3 and MDA-MB-231 cells were grown to 70-80% confluence, treated for 24 h with **2** and **3** at their respective  $IC_{50}$  values, and lysed as previously described [24]. Equal amounts of proteins were resolved on 15% SDS-polyacrylamide gel, transferred to a nitrocellulose membrane and probed with p-AKT, p-PTEN (Cell Signalling, Beverly, MA), AKT and p-mTOR specific antibodies (Santa Cruz, Biotechnology, CA, USA; all primary antibodies were used at 1:1000 dilution). In order to confirm equal loading and transfer, membranes were incubated with 1:1000 anti-GAPDH antibody (Santa Cruz, Biotechnology, CA, USA). Antigen-antibody complexes were detected by incubation of the membranes with peroxidase-coupled 1:5000 goat anti-rabbit or 1:10000 anti-mouse antibodies (Santa Cruz, Biotechnology, CA, USA) and revealed using the ECL System, as previously described [25] (Bio-Rad Laboratories, CA, USA).

### 2.12. Cell Cycle Analysis

MCF-7, MDA-MB-231 and SKBR-3 cells, seeded in 6-well plates at a density of  $1 \times 10^5$  cells/well, were treated with DMSO or **2** or **3** at  $IC_{50}$  for 36 hours. At the end of treatment, cell cycle analysis was performed using propidium iodide as previously described [26]. Samples were subjected to cytofluorimetric analysis using SONY SH800 Cell Sorter (Sony Corporation, Minato TYO, JP).

### 2.13. Transfection procedure and clone isolation

MCF-7 cells were grown up to 70-90% confluence and then transfected with PCMV-tag 2A PI3KCA-WT plasmid [27]. Briefly, MCF-7 cells were seeded into 24-well plates and cultured until the confluence reached 70-90%. Then, we dilute DNA (PCMV-tag 2A PI3KCA-WT plasmid and PCMV-tag 2A empty vector, separately) with serum-free medium to a final concentration of  $0.01 \mu\text{g}/\mu\text{L}$ . After that, we prepared two tubes (PCMV-tag 2A PI3KCA-WT plasmid and PCMV-tag 2A empty vector), for the respective cell lines, containing  $1 \mu\text{g}$  of DNA and diluted 3:1 with X-tremeGENE HP DNA (Roche, Basel, Switzerland) transfection reagent, previously allowed to equilibrate its temperature to  $+15$  to  $+25^\circ\text{C}$  and vortexed well. Then, the transfection reagent and DNA were incubated for 30 minutes at room temperature. Culture medium was removed and replaced with transfection complex in a dropwise manner, gently shaken and incubated. After 48 h of incubation, cells were trypsinized and different dilutions were made in a Petri dish to allow single colony formation. Normal medium for MCF-7 was supplemented with  $800 \mu\text{g}/\text{mL}$  of G418 antibiotic to mediate antibiotic selection. Medium was replaced every 6-7 days for 21 days, the time taken for colonies to integrate plasmid stably. Positive colonies were then trypsinized using specific rings containing trypsin to detach single colonies. In order to choose a clone that would properly overexpress the target protein, we performed an immunoblot analysis using anti PI3K p-110  $\alpha$  antibody (Abcam, Cambridge, MA).

### 2.14. Molecular docking calculations

Compounds **2** and **3** were docked into the published crystals of Phosphatidylinositol-3 Kinase alpha (PI3K $\alpha$ ) and Phosphoinositide-Dependent Protein Kinase 1 (PDK-1) whose X-ray

and 2PE0 [29], respectively. The X-ray solved structures were thus prepared by using Protein Preparation Wizard Schrödinger Suite 2018-4 [30] to add missing hydrogen atoms, to reconstruct incomplete side chains and assign favorable protonation states at physiological pH. In order to generate all the possible tautomers and ionization states at a pH value of  $7.0 \pm 2.0$ , **2** and **3** were prepared using LigPrep [31]. The obtained files were thus used for docking simulations by employing Grid-based ligand docking with energetics (GLIDE) [32]. During the docking process, full flexibility was allowed for the ligands while the protein was held fixed. The default force field OPLS\_2005 [33] and the standard precision (SP) protocol were employed using default settings. A cubic grid centered on the cognate ligands (that are NVP-BYL719 for 4JPS and 39Z for 2PE0, respectively) and having an edge of 10 Å for the inner box and 20 Å for the outer box was used. This computing protocol was validated by redocking the cognate ligands into their corresponding binding sites. In particular, cognate ligands moved back to the original positions with Root Mean Square Deviations (RMSD) accounting for all the heavy atoms equal to 0.282 Å and to 0.270 Å for NVP-BYL719 (better known as alpelisib) and 39Z, respectively.

### *2.15. Hemolysis assay*

All the study procedures with human fluids were approved by the Ethics Committee of the University of Calabria (Unical AOO1 Amministrazione Centrale, Doc. No.234 dated 14/01/2021). Fresh human blood from healthy volunteers was collected in sodium citrate tubes and centrifuged at 2000 rpm for 10 min to isolate red blood cells (RBCs) as a pellet. RBCs were exposed to 500 µM of **2** or **3** and incubated for up to 24 h at 37 °C. The release of hemoglobin was determined spectrophotometrically as previously described [34].

### *2.16. Plasma protein binding assay*

Fresh human blood from healthy volunteers was collected in sodium citrate tubes and centrifuged at 2000 rpm for 10 min to separate blood cells from the plasma fraction. Plasma fraction was then collected in a new tube and centrifuged at 2000 rpm for 10 min to completely

eliminate blood cells. Human plasma aliquots (199  $\mu\text{L}$ ) dispensed into vials were added with 1  $\mu\text{L}$  of **2** or **3** to obtain the final concentration of 500  $\mu\text{M}$ . Human plasma aliquots added with 1  $\mu\text{L}$  of Reboxetine to obtain the final concentration of 500  $\mu\text{M}$  were used as positive controls. Then, the samples were incubated at 37°C in a shaking water bath (60 oscillations/min approx.) for up to 24 h. At three different endpoints (0, 5 and 24 h), previously prepared samples were deproteinized using a 14 kDa cut-off centrifuge filter and the samples were subsequently subjected to HPLC analysis. The percentage of protein-bound compound were determined comparing the curve obtained from HPLC analysis after filtration to the calibration curves for **2**, **3** and Reboxetine in the range 50-500  $\mu\text{M}$ .

### 2.17. HPLC/MS measurements

Solvents ( $\text{H}_2\text{O}$  and  $\text{CH}_3\text{CN}$ ) were of HPLC/MS grade.  $\text{HCO}_2\text{H}$ , used as additive, was of analytical quality. The Agilent 1260 Infinity HPLC system was used. A C18 column (ZORBAX Extended-C18 2.1 x 50 mm, 1.8  $\mu\text{m}$ ) was employed. The flow was set at 0.4 mL/min. Column temperature was 30°C. Eluents were: Phase A, formic acid–water (0.1:99.9, v/v); Phase B, formic acid–acetonitrile (0.1:99.9, v/v). The following linear gradient from 5% to 95% B was applied from 0 to 10 min. 10  $\mu\text{L}$  was the injection volume. Total ion counts (TIC) were used to monitor the eluate. An Agilent 6540 UHD accurate-mass Q-TOF spectrometer was used to acquire mass spectra. A Dual AJS working in positive mode was employed as ESI source. Desolvation occurs at 300°C with  $\text{N}_2$  at a flow rate of 9 L/min. Nebulizer was set to 45 psig. The temperature of the Sheath gas was 350°C with a flow of 12 L/min. MS spectra were recorded in positive ion mode, with a potential of 3.5 kV and the fragmentor at 175 V. Mass range was 150–1000 m/z.

### 2.18. Statistical analysis

GraphPad-Prism 8 software was used to calculate the concentration giving 50% of inhibition ( $\text{IC}_{50}$ ) through nonlinear regression. All results were expressed as means  $\pm$  SD (standard deviation), taken over  $\geq$  three independent experiments, with  $\geq$  three replicates, unless otherwise stated. By using one-way analysis of variance (ANOVA) test, differences among means were tested for statistical significance.  $P$  value  $\leq$  0.05 was considered statistically significant.

3.1. *(Z)*-2-(2-oxopyrrolidin-3-ylidene)acetate derivatives **2** and **3** inhibit breast cancer cell survival and induce cell cycle arrest in G0/G1 phase and apoptotic cell death.

The antitumor potential of six newly synthesized alkyl *(Z)*-2-(2-oxopyrrolidin-3-ylidene)acetate derivatives **1-6** (Table 1) was first evaluated by assessing, through SRB assay, cell viability in three different tumor cell lines, namely the ER $\alpha$  positive MCF-7, triple negative MDA-MB-231, and Her2<sup>+</sup> SKBR-3 breast cancer cell lines. The investigated  $\alpha,\beta$ -unsaturated- $\gamma$ -lactam derivatives vary in hydrophobicity and bulkiness. Compounds **1-6** almost regularly show a lipophilicity range of about 1.7 log from the lowest for **1** (0.915) to the highest for **3** (2.603) log P values. Within the limits of the molecular property space examined, compound **4** (log P = 2.277) is the only *meta*-substituted N<sup>1</sup>-aryl derivative, and **5** (1.407) bears a methyl  $\alpha$  to the lactam N1. Apart from **6** (alkyl = Et), all compounds are methyl esters (alkyl = Me).

The compounds were first tested at 100  $\mu$ M. Among them, the most lipophilic compounds **2** and **3**, bearing the 1-(4-isopropylphenyl) or 1-(4-*tert*-butylphenyl) group bonded to nitrogen, respectively, turned out to be the most active ones, decreasing the viability of all the tested cancer cell lines (Figure 2A). Moreover, increasing concentrations (25, 50, 75 and 100  $\mu$ M) of **2** and **3** inhibited the cell viability of MCF-7, MDA-MB-231, and SKBR-3 cells, in a dose-dependent manner (Figure 2B). The IC<sub>50</sub> values for the active compounds are shown in Table 2, together with the values for doxorubicin used as positive control to assess the responsiveness of tumor cells. Noteworthy, albeit less potent than the anticancer drug doxorubicin, the antiproliferative activity of **2** and **3** was specific for cancer cells, since their IC<sub>50</sub> value ( $\gg$  100  $\mu$ M) on a non-tumorigenic breast epithelial cell line (MCF-10A) was remarkably higher than those determined in all the tested breast cancer cell lines.

With the aim of discriminating between the antiproliferative or cytotoxic effects of **2** and **3**, time-course experiments were carried out and cell proliferation was checked every day for 5 days. As shown in Figure 2C, starting from the second day, the proliferation curve of treated cells shows a much slower increment compared to that of the control cells, indicating a reduced

proliferation rate. After four days of treatment, cell death was observed as a steep decline in the proliferation curve compared to that of control cells. In order to understand whether the effects on growth observed after five days were due to prolonged exposure to the compounds or to a delayed consequence of activity in the first 24 hours, we modified the treatment. By treating for 1 day only with **2** or **3** and replacing the treatment with fresh medium for the remaining 4 days, similar results in the growth curves were obtained (Figure 2C). These outcomes highlight that the events responsible for the anticancer activity of the tested (*Z*)-2-(2-oxopyrrolidin-3-ylidene)acetates occur within the first 24 hours.

To determine whether the lower cell number was due to the induction of apoptotic death, we focused on DNA fragmentation, a late event in the apoptotic process [35], by comet assay. To this purpose, after treatment for five days with **2** or **3** at  $IC_{50}$  values, cells were suspended in agarose gel and rapidly added to frosted slides with a thin layer of agarose. Thereafter, slides were placed in a tank with lysis solution and then incubated in fresh alkaline buffer to allow the DNA to unwind. Following an electrophoresis run and DAPI staining, images of control cells showed a circular outline without any comet tail, which by contrast increased in length and size after treatment with **2** or **3** (Figure 2D), highlighting DNA fragmentation.



A

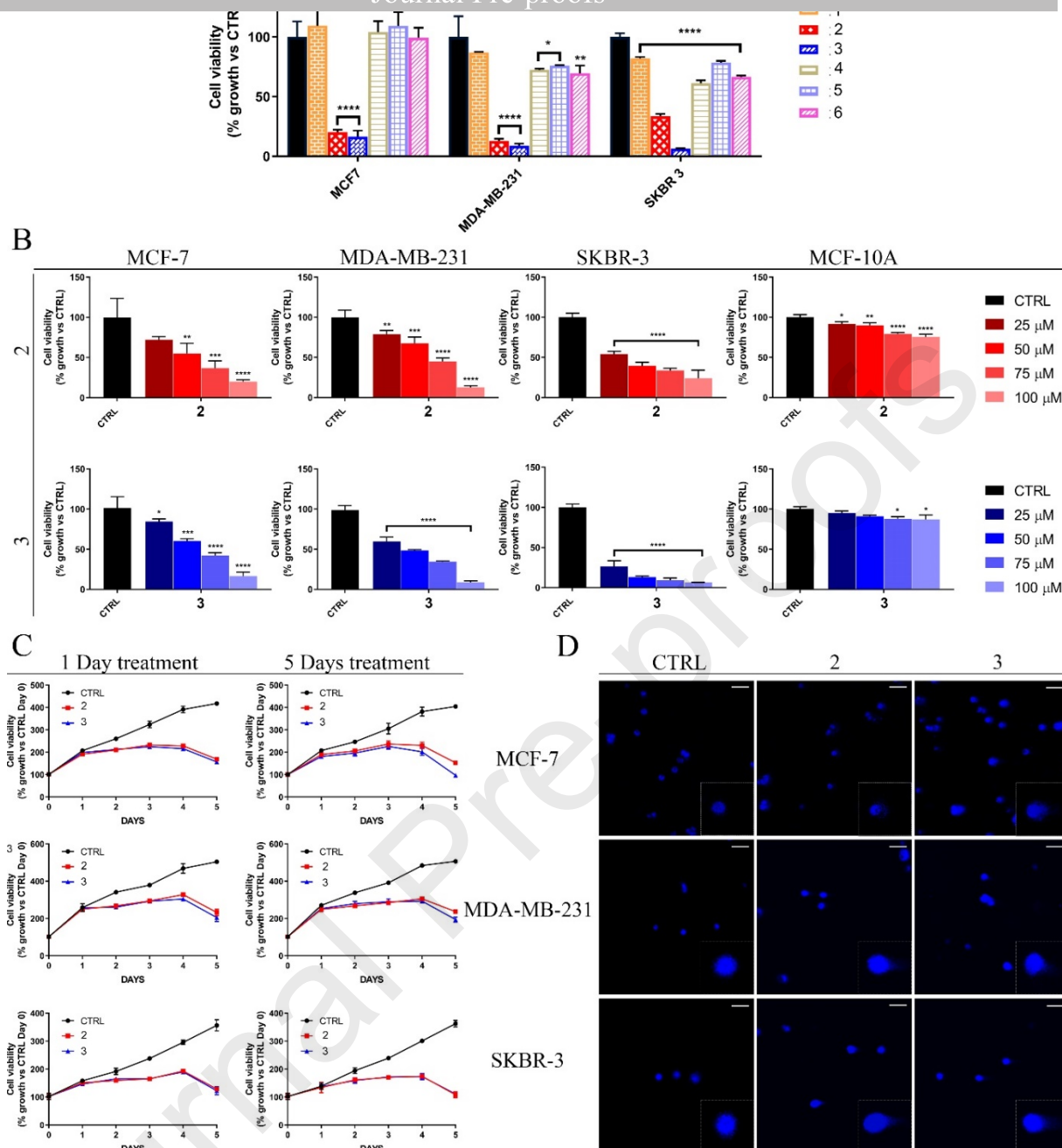


**Figure 2.** Compounds **2** and **3** exert antiproliferative and cytotoxic effects, inducing apoptotic death in breast cancer cells. Cell viability was assessed in breast cancer cells (MCF-7, MDA-MB-231 and SKBR-3) treated with 100 μM of alkyl (Z)-2-(2-oxopyrrolidin-3-ylidene)acetates **1-6** (A) or using different concentrations (from 25 μM to 100 μM) of **2** or **3** (B). (C) MCF-7, MDA-MB-231 and SKBR-3 cells treated at IC<sub>50</sub> values with **2** or **3** for 5 days either without interruption, or else replacing the medium after 24 hours. Cell viability was assessed day by day using SRB. (D) Breast cancer cells treated at IC<sub>50</sub> values with **2** or **3** for 5 days were subjected to the comet assay. DAPI was used to stain nuclei. Photographs of slides were taken at 20× on a fluorescent microscope, further magnifications of cells were obtained using 100× objective. Scale bar 25 μm. Values represent mean ± SD (n=3) from three independent experiments. \* P value < 0.05; \*\* P value < 0.01; \*\*\* P value < 0.001; \*\*\*\* P value < 0.0001.

The final event of the apoptotic process was further confirmed by TUNEL assay (Figure 3A,B,C) allowing quantification of the apoptotic cells (Figure 3D) in response to treatment with **2** or **3**, thus ultimately proving that both compounds induce apoptotic death in all tested cancer cell lines.

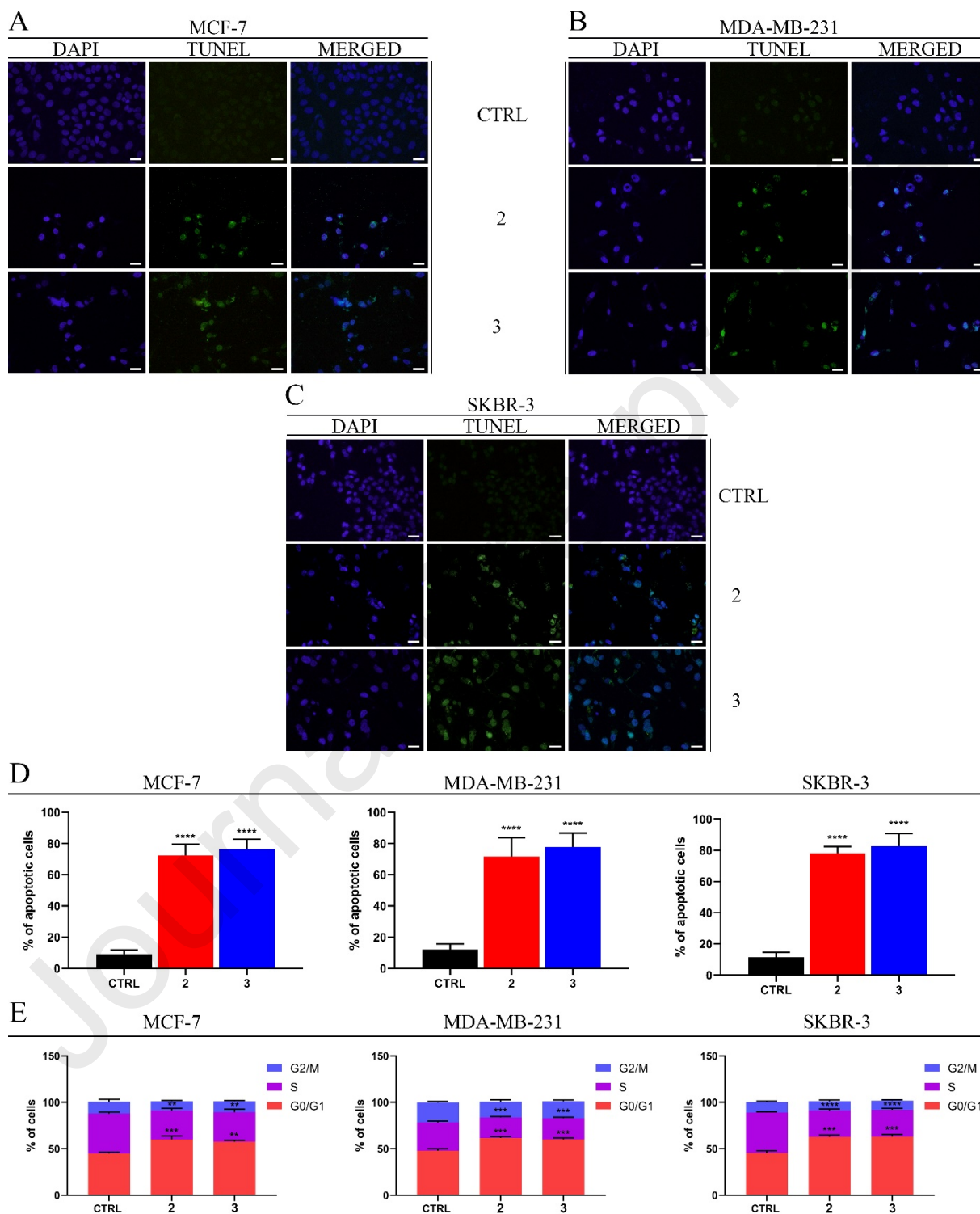


**Figure 3.** Compounds **2** and **3** induce apoptotic death confirmed by TUNEL assay and decrease proliferation rate of breast cancer cells inhibiting cell cycle. (A, B, C) MCF-7, MDA-MB-231 and SKBR-3 cells, respectively, treated at IC<sub>50</sub> values with **2** or **3** for 5 days were subjected to TUNEL assay. DAPI was used to stain nuclei.

Photographs of slides were taken at 20× on a fluorescent microscope. Scale bar 25 μm. **(D)** Histograms represent the % of apoptotic cells vs each control. **(E)** MCF-7, MDA-MB-231 and SKBR-3 cells treated, for 36 hours, with **2** or **3** at IC<sub>50</sub> were subjected to cell cycle analysis. Quantitative analysis of the percentage of cells arrested in different phases of the cell cycle was indicated. Values represent mean ± SD (n=3) from three independent experiments. \*\* *P* value < 0.01; \*\*\* *P* value < 0.001; \*\*\*\* *P* value < 0.0001.

We further investigated whether the two compounds **2** and **3** could affect cell cycle progression, as the causative event responsible for the observed antiproliferative effects. To this end, we performed the flow cytometric cell-cycle analysis by propidium iodide (PI) staining, on MCF-7, MDA-MB-231 and SKBR-3 cells after treatment with **2** or **3** at IC<sub>50</sub> values for 36 h. The results, shown in Figure 3E, clearly confirmed cell cycle arrest in the G1 phase, showing an increased percentage of cells in the G0/G1 phase (15%) with a concomitant decrease in the S phase (25%) in all the treated breast cancer cell lines. These findings proved that the biomolecular effects mediated by the two compounds in the first 24 hours of treatment culminate in cell cycle arrest.

**Table 2.** Cytotoxic activity of  $\gamma$ -lactams **2** and **3**.<sup>a</sup>

Cell Line		<b>2</b>	<b>3</b>	doxorubicin
MCF-7	<b>IC<sub>50</sub> (μM)</b>	<b>47.40</b>	<b>57.26</b>	<b>0.901</b>
	95% confidence interval	35.71 to 62.56	40.01 to 81.96	0.783 to 1.092
MDA-MB-231	<b>IC<sub>50</sub> (μM)</b>	<b>63.40</b>	<b>34.00</b>	<b>1.213</b>
	95% confidence interval	42.56 to 95.30	25.43 to 44.75	0.942 to 1.482
SKBR-3	<b>IC<sub>50</sub> (μM)</b>	<b>32.65</b>	<b>18.34</b>	<b>0.173</b>
	95% confidence interval	27.76 to 38.21	15.94 to 22.73	0.112 to 0.234
MCF-10A	<b>IC<sub>50</sub> (μM)</b>	<b>&gt; 100</b>	<b>&gt; 100</b>	<b>0.354</b>
	95% confidence interval	/	/	0.265 to 0.454

<sup>a</sup> Data are presented as IC<sub>50</sub> values (μM) and 95% confidence intervals obtained by nonlinear regression analysis of three independent experiments.

production

We performed immunofluorescent staining studies in order to determine whether the treatments are able to induce changes in  $\alpha$ -tubulin expression levels and distribution. A body of evidence highlights that  $\alpha$ -tubulin is involved in the proliferation process [36]. In this study, under normal culture conditions, MCF-7, MDA-MB-231 and SKBR-3 cells exhibited intense fluorescence due to the  $\alpha$ -tubulin immunoreactivity arrayed along the cytoplasm (Figure 4). After 24 h of treatment with compound **2** at its  $IC_{50}$  value, MCF-7, MDA-MB-231 and SKBR-3 cells showed a noticeable decrease in fluorescence. Similar results were obtained after treatment with **3** at its  $IC_{50}$  value (Figure 4).

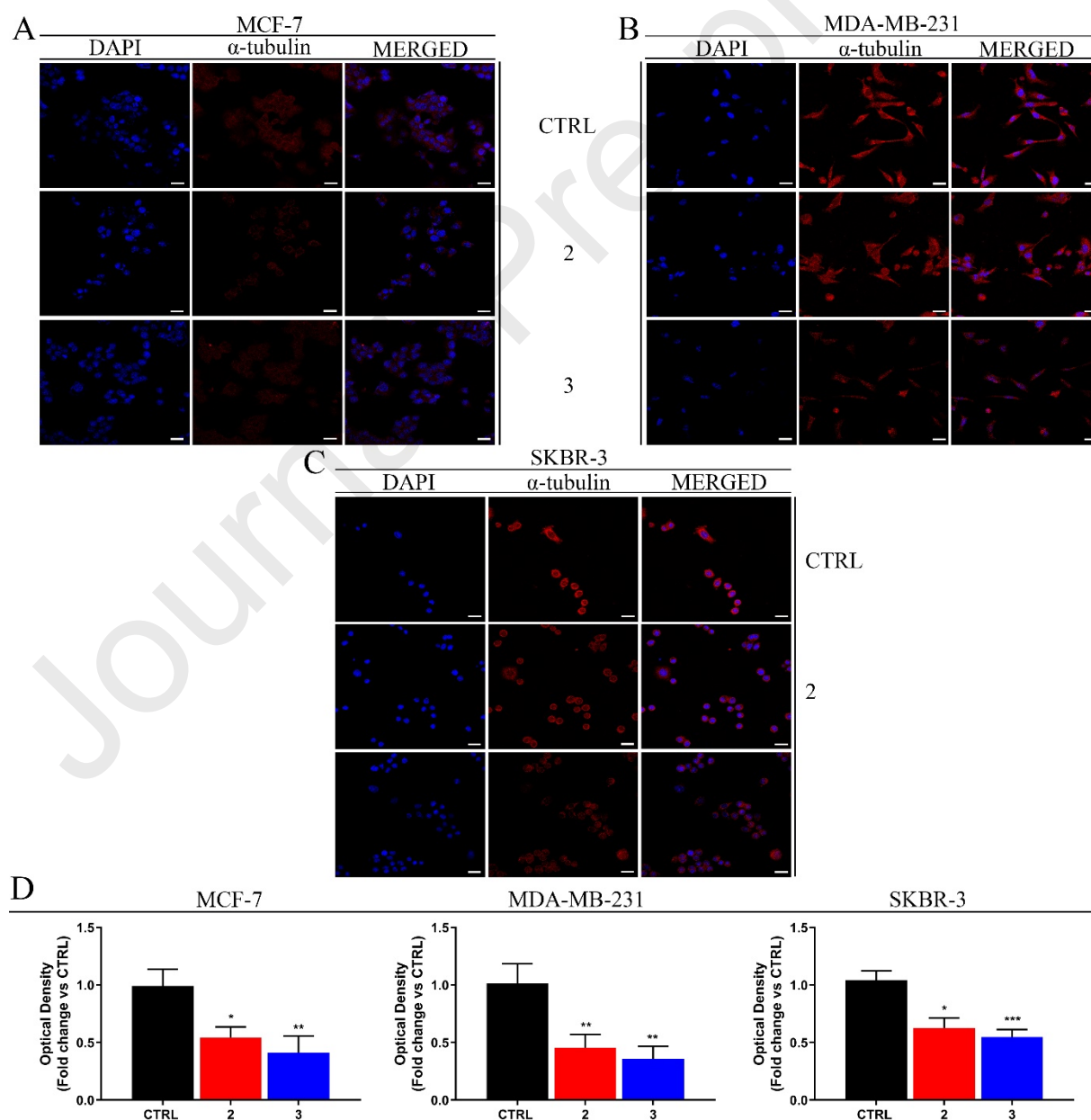


**Figure 4.** Compounds **2** and **3** decrease  $\alpha$ -tubulin immunoreactivity in breast cancer cells. Immunofluorescent

Journal Pre-proofs

staining of breast cancer cells (MCF-7 (**A**), MDA-MB-231 (**B**) and SKBR-3 (**C**)) treated with **2** or **3** at  $IC_{50}$  values for 24 h. DAPI was used to stain nuclei. Pictures were taken at  $20\times$  magnification. Scale bar 25  $\mu$ m. (**D**) Histograms represent the intensity of fluorescence as results of immunoreactivity of  $\alpha$ -tubulin in response to treatment with **2** or **3** compared to each control. Values represent mean  $\pm$  SD (n=3) of three independent experiments. \*  $P$  value < 0.05; \*\*  $P$  value < 0.01; \*\*\*  $P$  value < 0.001.

### 3.3. (Z)-2-(2-oxopyrrolidin-3-ylidene)acetate derivatives **2** and **3** affect malignant cancer hallmarks

The hallmarks of cancer comprise different biological abilities acquired during the multistep process of human tumorigenesis [37, 38]. They include enabling replicative immortality, inducing angiogenesis, activating invasion and metastasis, and producing cancer stem-like cells (CSCs).

First, we assessed whether compounds **2** and **3** could interact with the cancer's ability to produce colonies from single cells, a hallmark of an aggressive cancer phenotype. We used the colony formation assay that essentially tests every cell in the population for its ability to undergo "unlimited" division. As shown in Figure 5, the colony formation rate significantly decreased after treatment with **2** or **3** with respect to untreated cells, used as controls (Figure 5A). In addition, colony reduction was observed after one day of treatment, underlining that the biomolecular events responsible for the anticancer activity of (Z)-2-(2-oxopyrrolidin-3-ylidene)acetates occur within the first 24 hours of treatment. Secondly, due to the capacity of some cancer cells (i.e., triple-negative breast cancer cells characterized by a highly invasive nature) to promote metastasis through movement, we examined the ability of **2** and **3** to affect cell movement in wound-healing scratch assays. The experiments were performed on MCF-7, MDA-MB-231 and SKBR-3 cells, treated with **2** and **3** at  $IC_{50}$  values, for 24 h. Figure 5B shows that untreated cells in the respective cell lines, used as controls, invaded the wound area; conversely, after treatment with **2** or **3**, cell movement to close the gap was significantly reduced. These results suggest that both compounds are able to exert antimigratory effects in all

three of the breast tumor cell lines used. It is noteworthy that the most relevant effect was found in MDA-MB-231, the most aggressive cells tested.

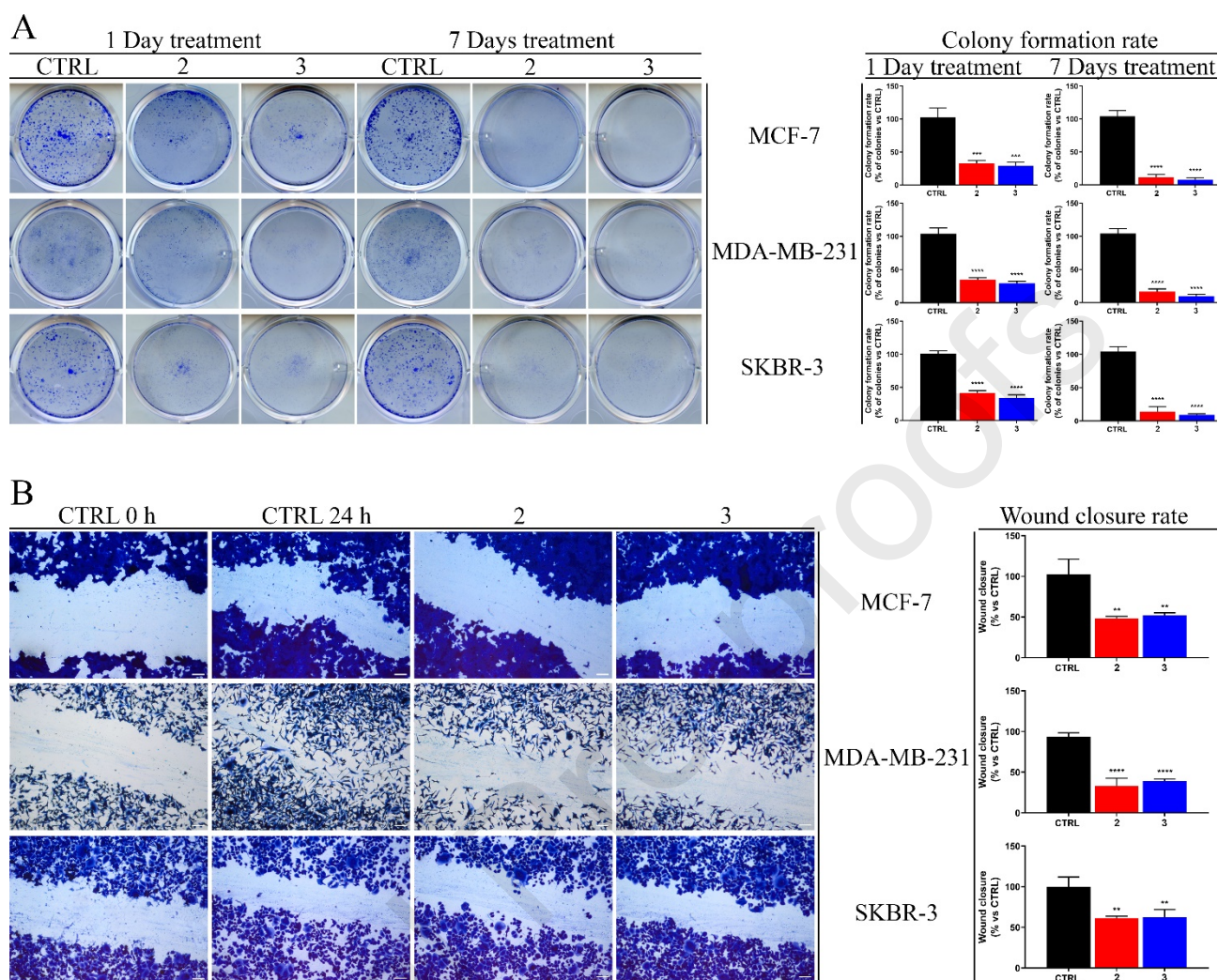


**Figure 5.** Compounds **2** and **3** decrease unlimited division and migratory effects in breast cancer cells. **(A)** Colony-formation assay in breast cancer cells (MCF-7, MDA-MB-231 and SKBR-3) treated with **2** or **3** at  $IC_{50}$  value either for 7 days or else for just one day, replacing the treatment with fresh medium after 24 hours. **(B)** Wound healing scratch assay in MCF-7, MDA-MB-231 and SKBR-3 treated with **2** or **3** at  $IC_{50}$  value for 24 h. Pictures were taken at  $10\times$  magnification. Scale bars  $50\ \mu\text{m}$ . Values represent mean  $\pm$  SD ( $n=3$ ) from three independent experiments. \*\*  $P$  value  $< 0.01$ ; \*\*\*  $P$  value  $< 0.001$ ; \*\*\*\*  $P$  value  $< 0.0001$ .

It is known that the tumor cell requires more nutrients for its growth due to its enhanced metabolism [39], and can therefore release several factors that lead to the formation of new vessels within the tumor in order to supply itself with nutrients and to extend itself to remote tissues. Consequently, we next wondered whether **2** and **3** could interfere in new vascular endothelium formation by evaluating what implication they might have in the release of metabolic factors by the tumor cells in the culture medium. The results showed that the

conditioned medium derived from breast cancer cells treated with **2** or **3** at IC<sub>50</sub> values for 24 h  
Journal Pre-proofs

was unable to induce new endothelial formation (Figure 6A), when used to culture endothelial cells, compared to a conditioned medium derived from untreated breast cancer cells (Figure 6A). Figure 6B displays the cell viability of Ea HY926 cells, under these experimental conditions.

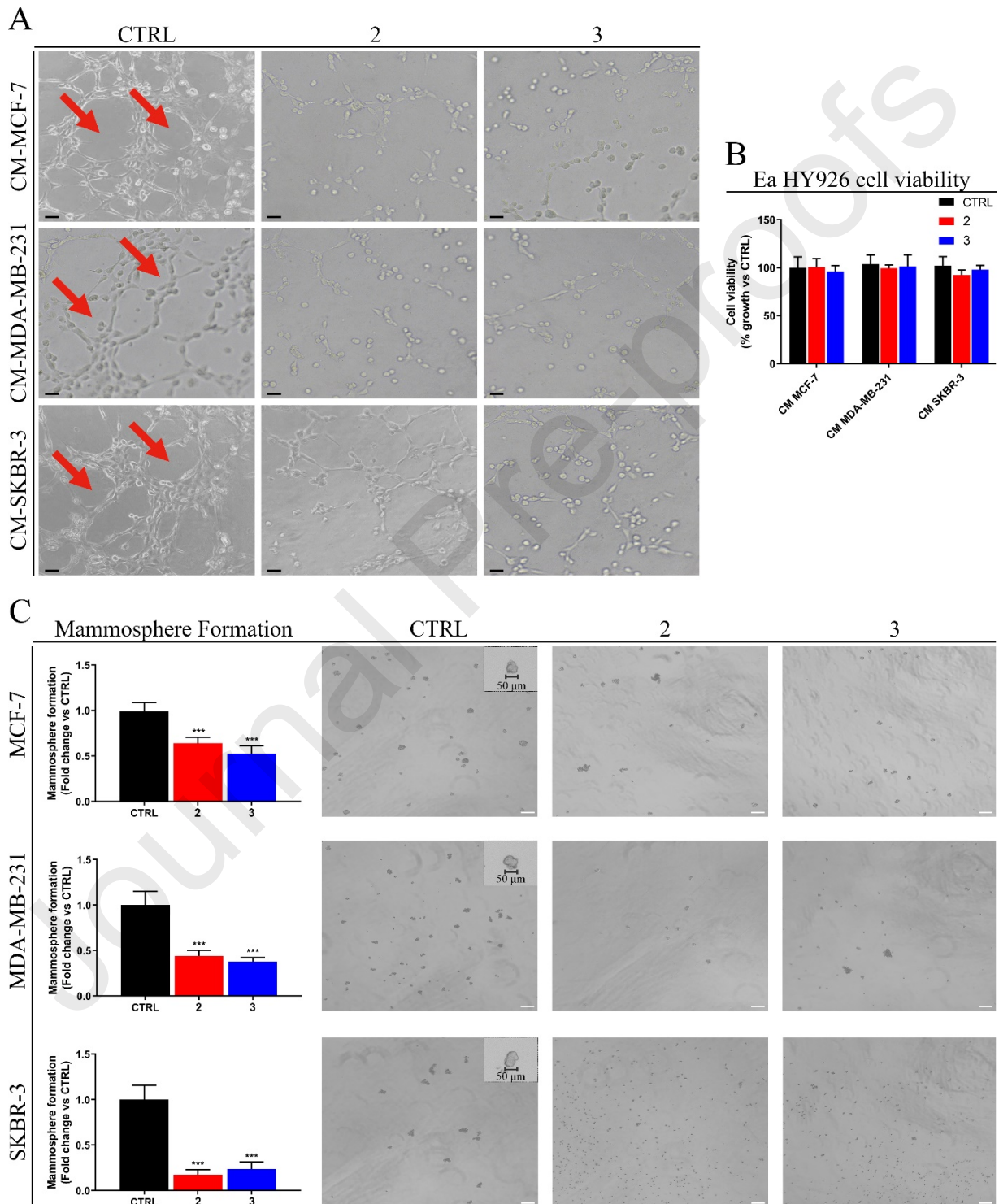


**Figure 6.** Compounds **2** and **3** target two cancer features, i.e. new vascular endothelium formation and CSC propagation. (A) Tube formation assay in human endothelial cells (Ea HY926) treated, for up to 24 h, with conditioned media (CM) from breast cancer cells treated with **2** or **3** at IC<sub>50</sub> value for 24 h. Conditioned media from

breast cancer cells treated with vehicle was used as control (CTRL). Pictures were taken at 20 × magnification.

Scale bars 25  $\mu$ m. Red arrows indicate newly formed vessels in the control cells. **(B)** Cell viability of human endothelial cells (Ea HY926) treated for 24 h with conditioned media (CM) from breast cancer cells treated with **2** or **3** at IC<sub>50</sub> value for 24 h. Conditioned media from breast cancer cells treated with vehicle was used as control (CTRL). **(C)** Mammosphere formation efficiency assay was performed on breast cancer cells MCF-7, MDA-MB-231 and SKBR-3 after treatment for 5 days with **2** or **3** at IC<sub>50</sub> value. Mammospheres were counted using an Olympus BX41 microscope and pictures were taken at 4 × magnification (with further magnifications at 10 ×). Scale bars 125  $\mu$ m. Values represent mean  $\pm$  SD (n=3) of three independent experiments. \*\*\* *P* value < 0.001.

Finally, we evaluated whether **2** or **3** were able to prevent the development of CSCs, a subpopulation of tumor cells responsible for therapy resistance and tumor recurrence [40]. Figure 6C shows that CSC formation and propagation were clearly reduced after exposure of MCF-7, MDA-MB-231, and SKBR-3 cell lines to **2** or **3** at IC<sub>50</sub> values for 5 days. Notably, this evidence demonstrates the ability of both compounds to target CSCs.

#### 3.4. *(Z)*-2-(2-oxopyrrolidin-3-ylidene)acetate derivatives **2** and **3** decrease AKT phosphorylation

It is known that the phosphatidylinositol 3-kinase (PI3K)/protein kinase B (AKT) (PI3K/AKT) signaling pathway plays an important role in cell proliferation and in apoptotic cell death reduction, as well as in inducing cell migratory effects and in controlling  $\alpha$ -tubulin expression levels [18, 41, 42]. The above results prompted us to investigate whether the PI3K/AKT signaling pathway could be a major target of **2** and **3**. An immunoblotting analysis of the main PI3K/AKT signaling pathway proteins, after treatment with **2** or **3** at IC<sub>50</sub> values for 24 h, was carried out in order to understand where the new derivatives were able to interfere with this signaling pathway. The phosphorylated form of AKT (p-AKT) is the pivot of the pathway controlling its downstream levels [42]. After 24 h of treatment, we observed a significant reduction in both AKT phosphorylation, at Ser473 residue (p-AKT S473), and mTOR (p-mTOR), the protein activated by AKT (Figure 7A).

A decreased AKT phosphorylation rate may be due to reduced availability of phosphoinositide 3,4,5-triphosphate (PIP3), which serves as the phosphate group donor in the



phosphorylation process. Since PIP3 levels are related to the activity of two enzymes (PI3K, responsible for its generation, as well as PTEN responsible for its degradation), we focused our attention on expression levels of p-PTEN, the inactive form of PTEN [41]. Immunoblotting analysis assessed on treated MCF-7, MDA-MB-231 and SKBR-3 cells (Figure 7A) revealed no changes in p-PTEN expression levels, in all tested breast cancer cells, suggesting that the activity of the enzyme, i.e. depriving the substrate, was not affected by the alkyl (*Z*)-2-(2-oxopyrrolidin-3-ylidene)acetate derivatives. In order to investigate the involvement of growth factor receptor (RTK, the first protein in the PI3K/AKT pathway), we evaluated, by SRB assay, the effects of a co-treatment with hEGF 20 ng/mL and **2** or **3** (at IC<sub>50</sub> value), in all tested breast cancer cell lines. We found that co-treatment with hEGF could not neutralize the effects of the compounds (Figure 7B). These results confirm that RTK activity is unrelated to the decreased AKT phosphorylation rate induced by **2** or **3**.

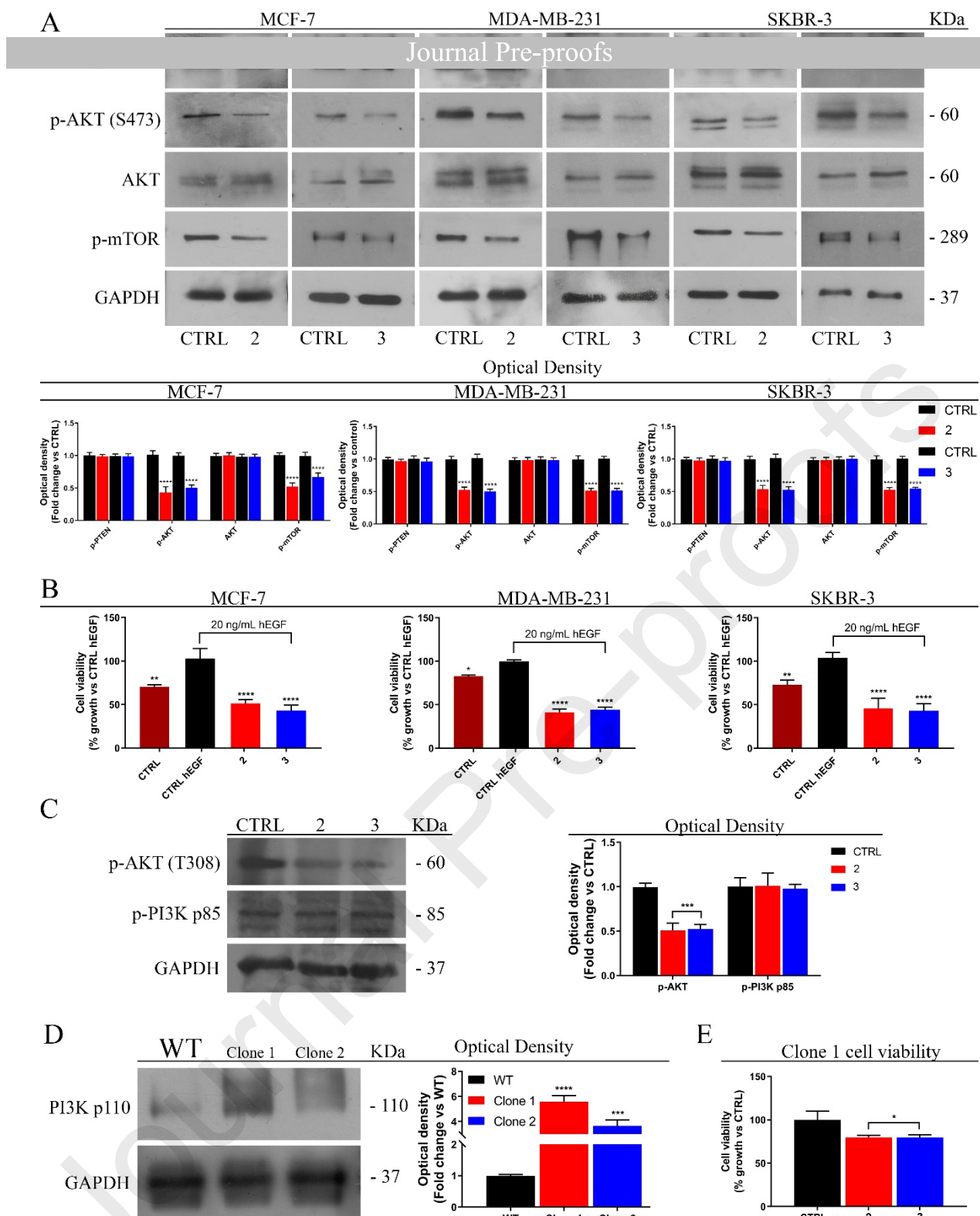


**Figure 7.** Compounds **2** and **3** act on the PI3K/AKT signaling pathway. **(A)** Immunoblot analysis of the main proteins involved in the PI3K/AKT pathway after treatment with **2** or **3** at  $IC_{50}$  values for 24 h. Optical densities of their expression levels by densitometry are also shown. **(B)** Cell viability assay in breast cancer cells co-treated with **2** or **3** at  $IC_{50}$  values and 20 ng/mL hEGF for 5 days. **(C)** Immunoblot analysis of p-AKT (T308) and p-PI3K p85 after treatment of MCF-7 cells with **2** or **3** at  $IC_{50}$  value for 24 h. Optical densities of their expression levels by densitometry are also shown. **(D)** Immunoblot analysis of PI3K p110 in transfected MCF-7 cells with respect to MCF-7 cells transfected with empty vector (WT). Optical densities of the different expression levels by

densitometry are also shown. **(E)** Viability assay of MCF-7 cells transfected with PCMV-tag 2A PI3KCA-WT (Clone 1) treated with **2** or **3** at its IC<sub>50</sub> for 5 days. Values represent mean  $\pm$  SD (n=3) from three independent experiments. \* *P* value < 0.05; \*\*\* *P* value < 0.001; \*\*\*\* *P* value < 0.0001.

Taking this outcome into account, we were able to delimit the target of **2** and **3** to two important enzymes of this pathway, PI3K and PDK-1. PI3K plays a critical role in the phosphorylation of PIP<sub>2</sub> to PIP<sub>3</sub>; the latter is the substrate used by the active PDK-1 (p-PDK-1) to phosphorylate AKT. Therefore, we assessed whether PDK-1, controlled by PI3K, was blocked after treatment with **2** or **3**.

As shown in Figure 7C, MCF-7 cells, treated with the tested compounds at IC<sub>50</sub> for 24 h, evidenced a severe decrease in AKT phosphorylation at Thr308 (p-AKT T308). Since this phosphorylation is directly mediated by PDK-1, this suggests that the signaling pathway interruption could be due to a decreased activity of PDK-1 and/or to a decreased activity of PI3K, the enzyme needed to activate PDK-1. Interestingly, the levels of the active form of PI3K (in its phosphorylated form, p-PI3K p85) were stable after treatment with the  $\alpha$ -methylene- $\gamma$ -lactam derivatives, further confirming that the upstream part of the signaling pathway was not modified by treatment and ultimately indicating PDK-1 and PI3K as targets of **2** and **3**.

To shed further light on targets of **2** and **3**, we evaluated whether overexpression of the catalytic subunit of PI3K was able to revert the effects induced by both compounds. We stably transfected MCF-7 cells with PCMV-tag 2A PI3KCA-WT construct. Stable clone was isolated using G-418 antibiotic selection, subjected to immunoblot analysis to confirm overexpression (Figure 7D) and then exposed to treatment with **2** or **3**. Figure 7D shows that MCF-7 PI3KCA-WT cells were less sensitive to treatment compared to MCF-7 cells transfected with empty vector (WT), confirming that the PI3K enzyme could be the target of **2** or **3** but, at the same time, highlighting the possible involvement of PDK-1.

*3.5. Molecular docking of the lipophilic methyl (Z)-2-(2-oxopyrrolidin-3-ylidene)acetate derivatives 2 and 3 to PI3K and PDK-1 binding sites*

within the binding sites of PI3K and PDK-1, molecular docking simulations were carried out. As far as PI3K is concerned, the X-ray structure complex (PDB code: 4JPS) at a resolution of 2.2 Å was employed [28]. Notably, the complex includes as a cognate ligand NVP-BYL719, a potent and selective PI3K $\alpha$  inhibitor, recently approved under the name alpelisib as a drug for the treatment of breast cancer [42].

Based on this wealth of information, **2** and **3** were docked on the chain A of 4JPS in an attempt to experience the same molecular interactions engaged by alpelisib with residues Gln859 and His855, the former in particular clearly playing a role for selectivity, and with residues Ile848, Ile800, Pro778 and Lys802 forming a hydrophobic cavity, which is important for affinity. As shown on panel (A) of Figure 8, top-scored docking poses of **2** and **3** were both effective in engaging interactions with Gln859, the key residue for selectivity, as observed for alpelisib. On the other hand, the docking pose of **3** was just slightly better than that of **2** at filling the hydrophobic cavity with its bulkier *t*-butyl group but not as long as alpelisib, which is a three-ring compound with a central 1,3-thiazole core. In fact, the hydrophobic cavity remains not totally filled by **2** and **3**, this likely being the cause of their lower docking scores of  $-7.088$  kcal/mol and  $-6.785$  kcal/mol, respectively, compared to that of alpelisib of  $-12.136$  kcal/mol. However, the effective binding potential calculated in terms of ligand efficiency (LE), which is a better accepted indicator of compound quality for prospective drug design [43], shows very similar LE values for **2**, **3** and alpelisib (reported in kcal/mol per heavy atom), of  $-0.354$ ,  $-0.323$  and  $-0.405$ , respectively.

As far as PDK-1 is concerned, the X-ray structure complex (PDB code: 2PE0) at a resolution of 2.35 Å was employed [29]. Interestingly, the complex's cognate ligand, 39Z, shares a certain degree of molecular similarity ( $> 0.6$ ) with the newly investigated compounds **2** and **3**. As reported elsewhere [29], a network of hydrogen bonds with hinge residues Ser160 and Ala162 is relevant for PDK-1 inhibition, along with specific interactions with key selectivity residues Thr222 e Lys111. As shown in panel (B) of Figure 8, top-scored docking

poses of **2** and **3** approached Lys111 via a water bridge hydrogen bond, joining the protonated nitrogen atom of Lys111 to their oxygen atoms on the acetyl ester head. A substantially similar posing is also evident when comparing **2** and **3** vs. 39Z (see black wireframe on panel (B) of Figure 8). In parallel, the scoring of **2** and **3**, equal to  $-6.709$  and  $-6.722$  kcal/mol, respectively, is to a large extent comparable to that observed for 39Z, of  $-7.601$  kcal/mol. This trend reflects the closer LE values calculated for **2** and **3** and 39Z, of  $-0.336$ ,  $-0.319$  and  $-0.383$ , respectively. Based on this investigation, **2** and **3** can be considered two excellent molecular hits for preventing PI3K and PDK-1 from functioning, as both can recognize and, more importantly, interact with selectivity residues although with moderate affinity. In this respect, the molecular decoration of the aromatic ring and the insertion of suitable chemical spacers could be a viable option to better sample the small hydrophobic cavity of PI3K as well as the hinge region of PDK-1 in an attempt to enhance affinity towards these pharmacological targets.

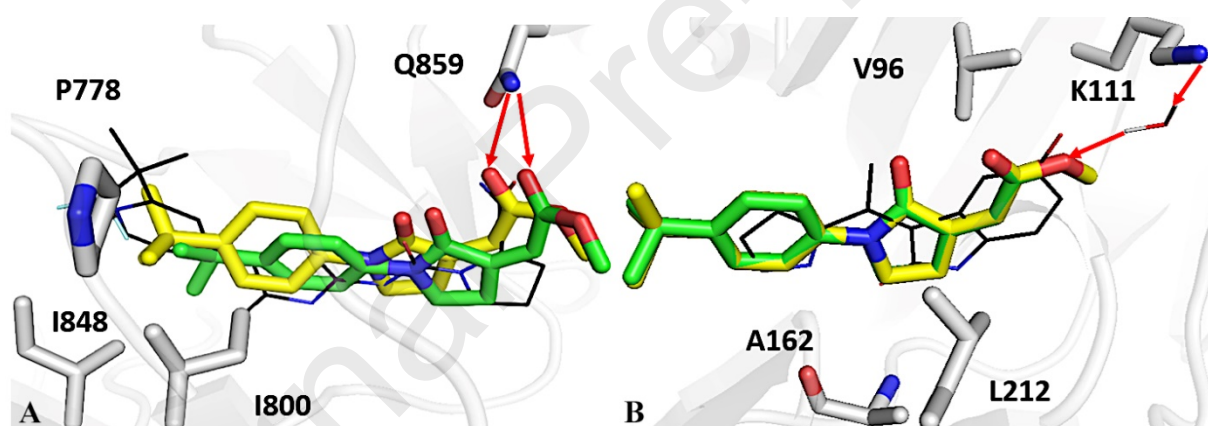


**Figure 8.** Zoomed in view at the PI3K (PDB entry 4JPS) and PDK-1 (PDB entry 2PE0) binding sites in panels (A) and (B), respectively. Top-scored docking poses for **2** and **3** are rendered as green and yellow sticks, respectively while red arrows indicate hydrogen bonds. The cognate ligands, which are alpelisib for PI3K and 39Z for PDK-1, and the functional water molecule are depicted in black and color-type wireframes, respectively.

### 3.6. Interaction studies with human blood

To evaluate the translational potential of our compounds, we performed two different assays using peripheral blood from healthy volunteers. First, we assessed the hemolysis rate induced by **2** and **3**. For this purpose, red blood cells (RBCs) from the peripheral blood of healthy volunteers were exposed to  $500 \mu\text{M}$  **2** or **3**, for 1 or 24 h, to evaluate the hemolysis rate

induced by these two compounds. The results highlighted no hemolytic effects (< 5 %) at tested concentrations compared to 0.1% Tween-100 used as control of complete hemolysis (Figure 9A).

Subsequently, we evaluated the binding of both derivatives to plasma proteins, which is another important parameter to identify the ability of a compound's free fraction to cause activity in the organism. To this end, plasma fraction was obtained from the peripheral blood of healthy volunteers and incubated with 500  $\mu$ M **2**, **3** or reboxetine (positive control) for 5 h or 24 h. The samples were filtered to remove proteins and to collect the free fraction of the compounds unbound to plasma proteins and then analyzed by HPLC. As shown in Figure 9B, the percentage of plasma protein-bound compounds calculated respect to the standard curve obtained for **2**, **3** and reboxetine in the range 50-500  $\mu$ M, evidenced high binding power to plasma proteins.

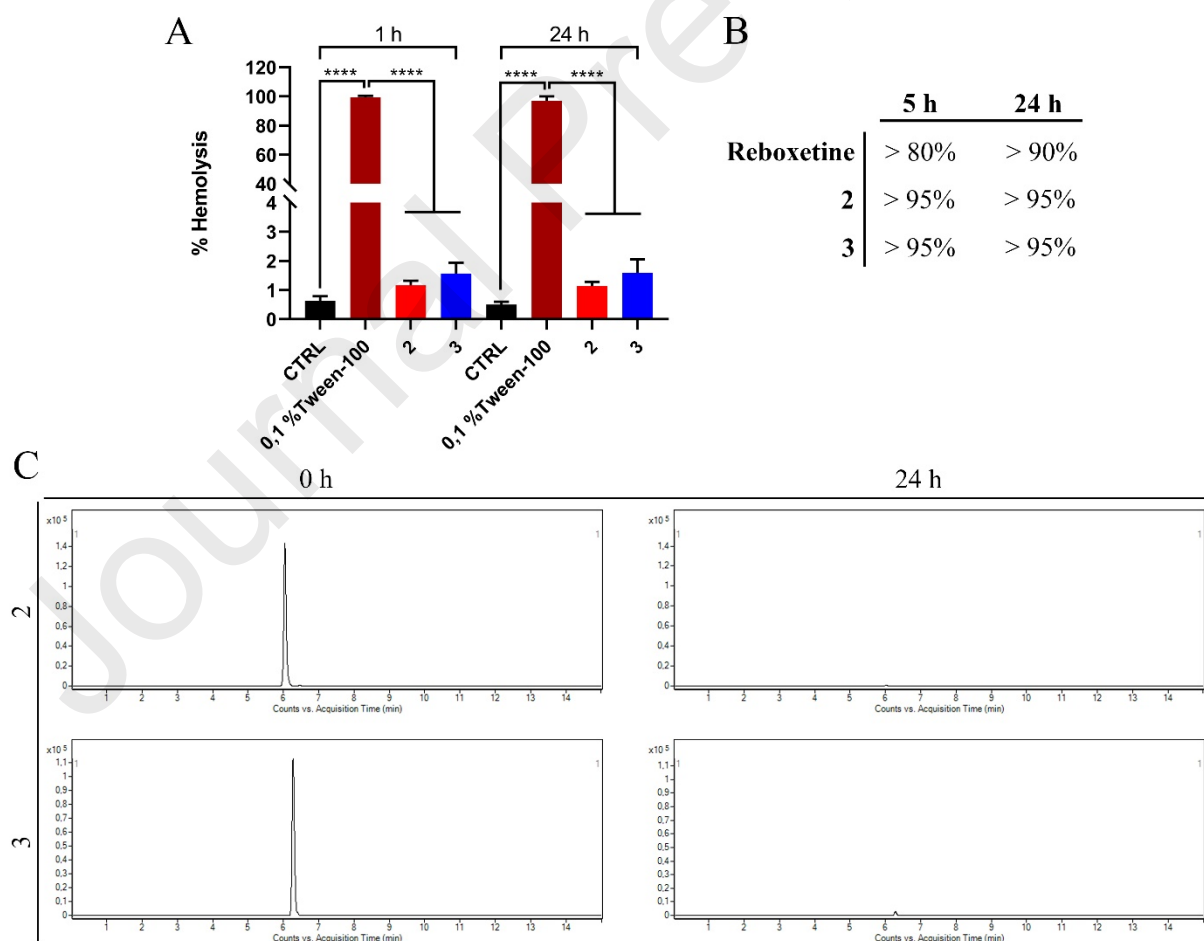


**Figure 9.** Compounds **8** and **9** interact with plasma proteins and did not exert hemolytic effects. **(A)** Hemolysis assay on RBCs treated with DMSO (CTRL), 0.1% Tween-100, 500 $\mu$ M **2** or 500 $\mu$ M **3** for 1h or 24 h. Histograms

represent the relative percentage of hemolysis from three different experiments, each performed with triplicate samples. (B) Protein binding assay on plasma protein treated with 500  $\mu$ M **2** or 500  $\mu$ M **3** up to 24 h. Data represent the relative percentage of **2** or **3** bound to the proteins coming from HPLC analysis of three different experiments, each performed with triplicate samples. (C) Representative HPLC analysis of free fractions in human plasma of **2** and **3**. Values represent mean  $\pm$  SD (n=3) of three independent experiments. \*\*\*\**P* value < 0.0001.

#### 4. Discussion

Six alkyl (*Z*)-2-(2-oxopyrrolidin-3-ylidene)acetate derivatives **1-6** (Table 1), selected from a focused library recently synthesized by Gabriele's group using an innovative sustainable method based on catalytic carbonylation of homopropargylic amines [13], were evaluated *in vitro* for their cytotoxic effects in three different breast cancer cell models, namely the ER $\alpha$  positive MCF-7, triple negative MDA-MB-231, and Her2+ SKBR-3 breast cancer cell lines. The biological and computational findings of this study adds a wealth of knowledge regarding the cytotoxic potential of the  $\alpha$ -methylene- $\gamma$ -lactam moiety, which has been far less explored in literature than the corresponding  $\gamma$ -lactone scaffold [13]. The most lipophilic congeners **2** and **3**, bearing the 4-isopropylphenyl or 4-*tert*-butylphenyl group, respectively, bonded to nitrogen, were found to be the most active ones within the series. These compounds decreased proliferation in all the tested breast cancer lines, though at concentrations one order of magnitude higher than those of doxorubicin, used as positive control. However, it is noteworthy that, unlike doxorubicin, they showed no antiproliferative activity in the non-tumorigenic MCF-10A epithelial breast cell line, even at 100  $\mu$ M, a concentration 2-3 times higher than that used in tumor cells.

Subsequently, the anti-proliferative effect induced by the two compounds was better characterized using a time-course study that, at first, revealed a decreased cell proliferation rate, as confirmed by the cell cycle arrest in the G0/G1 phase, and then, cytotoxic effects and cellular death, in all breast cancer cell lines tested. Cell death was further confirmed by DNA fragmentation, a late event of apoptosis, evidenced after exposure of the all tested cell lines to **2** or **3**.

eradication of the neoplastic pathology; indeed, in the last few years, microenvironment and cancer hallmarks are becoming increasingly more important in the discovery of effective anticancer agents [44-46]. The selectivity of compounds **2** and **3** toward cancer cells prompted us to evaluate different cancer hallmarks characterizing tumor progression and aggressiveness. Using colony formation and wound healing assays, we evaluated the ability of cancer cells to survive and replicate unlimitedly starting from single cells, as well as their ability to move and invade nearby structures. Interestingly, our findings proved that all the tested breast cancer cells, after exposure to **2** or **3**, showed sharp decreases in the above features.

Cancer cells are also characterized by metabolic reprogramming associated with the increased demand for nutrients that drives tumor propagation; indeed, tumors require catabolites to produce ATP and generate biomass [39]. Cells within the tumor have a metabolism that varies according to the availability of nutrients spanning from a mainly glycolytic state to a phenotype dependent on oxidative phosphorylation [22, 39, 47]. To cope with this continuous demand for nourishment, the cancer cell promotes the formation of new blood vessels within the tumor in order to obtain nutrients, as well as to allow cancer cells to spread into the bloodstream, thus prompting the onset of distant metastases [21]. Therefore, drugs that act on endothelial growth may also be crucial in clinical practice by acting as adjuvants to normal therapies [48]. In this context, we demonstrated that Ea Hy926, endothelial cells, widely used for evaluating angiogenesis, showed a marked reduction in new vessel formations, when grown using conditioned media from breast cancer cells exposed to **2** or **3** to induce tube formation.

Both metabolic rearrangement and new blood vessel formation also play a key role in the formation and propagation of cancer stem-like cells (CSCs), a subpopulation of tumor cells mainly responsible for cancer resistance, recurrence and metastasis, that is a driving force of tumorigenesis [49]. CSCs are characterized by high metabolic flexibility, which allows them to switch from the glycolytic to phosphorylative pathways according to the energy needs of the malignant cell [50]. Current anticancer drug research aims at disclosing drugs that can hit the



proved that **2** and **3** decrease CSC formation and propagation.

Overall, our findings prompted us to hypothesize the PI3K/AKT pathway as target of the newly synthesized compounds. Many types of cancer are highly dependent on this pathway [51, 52] and its overactivation is related to poor prognosis and higher aggressiveness [18]. Several reports highlighted that diverse inhibitors of this signaling pathway are characterized by the same effects induced by **2** and **3**. For instance, NVP-BEZ235 and NVP-BYL719, act by promoting antiproliferative effect (mediated by cell-cycle impairment with cell accumulation in the G0/G1 phase), apoptotic death and decrease of cell migration in various cancer types [28, 53-55]. Furthermore, GSK2126458, in preclinical studies, proved to be a promoter of cell cycle arrest in phase G1, inducing antiproliferative effects and apoptotic cell death, as well as targeting the main cancer hallmarks [31, 48, 56]. Moreover, the effects exerted by **2** and **3** on  $\alpha$ -tubulin could be related to PI3K/AKT pathway perturbation, since several studies highlight the link between this signaling pathway and microtubule homeostasis [57, 58].

Our hypothesis would seem further supported by the IC<sub>50</sub> values for **2** and **3** found in the tested breast cancer cells which highlighted greater or lesser sensitivity to the treatment related to their dependence on this pathway.

In particular, MCF-7 cells are endowed with a mutation related to high activation of the signaling pathway [59]; indeed, this mutation regulates the activation-inactivation state of the PI3K enzyme. SKBR-3 cells are characterized by marked activity of the PI3K/AKT pathway [60] while MDA-MB-231 cells exhibit constitutive overexpression of the RAS protein, an intermediate in the MAPK cascade, which by phosphorylating PI3K, promotes the activation of the PI3K/AKT signaling pathway, regardless of RTK activation [61]. In this regard, our results showed a marked effect on the part of compounds **2** and especially **3** both in the SKBR-3 and in the MDA-MB-231 cell lines.

Starting from this hypothesis, we demonstrated that **2** and **3** induce their effects by acting on this signaling pathway; indeed, immunoblot analysis revealed the main proteins involved,

levels were stable, while RTK receptor was unaffected by exposure to **2** or **3**. These results led us to suggest PI3K and PDK-1, two intermediate enzymes of the PI3K/AKT pathway, as targets of **2** and **3**. Furthermore, by overexpressing the catalytic subunit of PI3K, we observed a reduction in the effects mediated by **2** and **3**. However, the lack of complete restoration of cell viability suggests a possible implication of PDK-1. Based on these findings, we carried out *in silico* docking analyses to evaluate whether PI3K and PDK-1 could represent putative targets for **2** and **3**. Interestingly, our molecular docking calculations indicate that **2** and, even better, **3** could effectively target PI3K and PDK-1 binding sites by interacting with a number of key residues, suggesting that (Z)-2-(2-oxopyrrolidin-3-ylidene)acetates can be considered a promising chemotype for designing novel anticancer drugs interfering with the PI3K/AKT signaling pathway. In this respect, within the limits of the property space examined, it can be deduced that small branched alkyls at the *para* position of the 1-phenyl group do increase the anticancer potential, whereas the herein reported docking models of **2** and **3** in the PI3K (pdb 4JPS) and PDK-1 (pdb 2PE0) binding sites should support the molecular design of suitably decorated  $\alpha$ -methylene- $\gamma$ -lactam derivatives in order to better fit the two biological drug targets.

Finally, our data proved both the absence of significant toxic effects on red blood cells (RBCs) and interactions with plasma proteins, that may support a safe use of these molecules for future studies *in vivo*, and also indicate **2** and especially **3** as hits for further hit-to-lead optimization studies, laying the foundation for a novel class of potential anticancer chemotherapeutics.

#### **CRedit authorship contribution statement**

**Matteo Brindisi:** Conceptualization, Investigation, Methodology, Data curation, Writing - original draft, Writing - review & editing. **Luca Frattaruolo:** Conceptualization, Investigation, Methodology, Writing - review & editing. **Raffaella Mancuso:** Conceptualization, Investigation, Writing - review & editing. **Antonio Palumbo Piccionello:** Investigation, Data curation, Writing - review & editing. **Ida Zicarelli:** Investigation, Writing - review & editing. **Marco Catto:** Investigation, Writing - review & editing. **Orazio Nicolotti:** Investigation, Data

Writing - original draft, Writing - review & editing. **Bartolo Gabriele**: Conceptualization, Supervision, Writing - review & editing. **Anna Rita Cappello**: Conceptualization, Data curation, Supervision, Writing - original draft, Writing - review & editing.

### **Declaration of competing interest**

The authors declare no conflict of interest.

### **Acknowledgements.**

C.D.A. and M.C. acknowledge the financial support of the Italian Ministry of Education, Universities and Research (PRIN, Grant 201744BNST\_004). O.N. acknowledges the “4FRAILITY e Sensoristica intelligente, infrastrutture e modelli gestionali per la sicurezza di oggetti fragili”, codex ARS01\_00345.

### **References**

- [1] R.L. Siegel, K.D. Miller, A. Jemal, Cancer statistics, 2015, *CA Cancer J Clin* 65(1) (2015) 5-29.
- [2] S. Friberg, A. Nystrom, Cancer Metastases: Early Dissemination and Late Recurrences, *Cancer Growth Metastasis* 8 (2015) 43-9.
- [3] M. Majidinia, M. Mirza-Aghazadeh-Attari, M. Rahimi, A. Mihanfar, A. Karimian, A. Safa, B. Yousefi, Overcoming multidrug resistance in cancer: Recent progress in nanotechnology and new horizons, *IUBMB Life* 72(5) (2020) 855-871.
- [4] B. Armentano, R. Curcio, M. Brindisi, R. Mancuso, V. Rago, I. Zicarelli, L. Frattaruolo, M. Fiorillo, V. Dolce, B. Gabriele, A.R. Cappello, 5-(Carbamoylmethylene)-oxazolidin-2-ones as a Promising Class of Heterocycles Inducing Apoptosis Triggered by Increased ROS Levels and Mitochondrial Dysfunction in Breast and Cervical Cancer, *Biomedicines* 8(2) (2020).
- [5] M. Bonesi, M. Brindisi, B. Armentano, R. Curcio, V. Sicari, M.R. Loizzo, M.S. Cappello, G. Bedini, L. Peruzzi, R. Tundis, Exploring the anti-proliferative, pro-apoptotic, and antioxidant properties of *Santolina corsica* Jord. & Fourr. (Asteraceae), *Biomed Pharmacother* 107 (2018) 967-978.
- [6] P.A. Jackson, J.C. Widen, D.A. Harki, K.M. Brummond, Covalent Modifiers: A Chemical Perspective on the Reactivity of alpha,beta-Unsaturated Carbonyls with Thiols via Hetero-Michael Addition Reactions, *J Med Chem* 60(3) (2017) 839-885.
- [7] J.H.C. II, R.E. Moore, The structures of pukeleimides A, B, D, E, F, and G, *Tetrahedron Letters* 20(22) (2001) 2007-2010.
- [8] N. T., H. Y., M. O., N. K., Total syntheses of (±)-anantine and (±)-isoanantine via thiyl radical addition-cyclization reaction, *Chemical and Pharmaceutical Bulletin* 41(1) (1993) 217-219.
- [9] H.V. Dodou, A.H.M. Batista, S.C. Medeiros, G.W.P. Sales, M.L. Rodrigues, P.I.O. Pereira, P.C.N. Nogueira, E.R. Silveira, T.B. Grangeiro, N.A.P. Nogueira, Violacein antimicrobial activity on *Staphylococcus epidermidis* biofilm, *Nat Prod Res* 34(23) (2020) 3414-3417.

alkylidene-gamma-lactones and lactams, *J Med Chem* 48(10) (2005) 3516-21.

[11] A. Albrecht, J.F. Koszuk, J. Modranka, M. Rozalski, U. Krajewska, A. Janecka, K. Studzian, T. Janecki, Synthesis and cytotoxic activity of gamma-aryl substituted alpha-alkylidene-gamma-lactones and alpha-alkylidene-gamma-lactams, *Bioorg Med Chem* 16(9) (2008) 4872-82.

[12] H. Ikuta, H. Shirota, S. Kobayashi, Y. Yamagishi, K. Yamada, I. Yamatsu, K. Katayama, Synthesis and antiinflammatory activities of 3-(3,5-di-tert-butyl-4-hydroxybenzylidene)pyrrolidin-2-ones, *J Med Chem* 30(11) (1987) 1995-8.

[13] R. Mancuso, I. Ziccarelli, M. Brindisi, A.C. D., L. Frattaruolo, F. A., D.C. N., A.R. Cappello, B. Gabriele, A Stereoselective, Multicomponent Catalytic Carbonylative Approach to a New Class of  $\alpha,\beta$ -Unsaturated  $\gamma$ -Lactam Derivatives, *Catalysts* 11(2) (2021) 227.

[14] R. De Marco, G. Mazzotti, A. Greco, L. Gentilucci, Heterocyclic Scaffolds in the Design of Peptidomimetic Integrin Ligands: Synthetic Strategies, Structural Aspects, and Biological Activity, *Curr Top Med Chem* 16(3) (2016) 343-59.

[15] J. Fu, M. Lindvall, J.R. Manning, G. McEnroe, A.G. Novartis, Novel Dihydroisoxazole Compounds and Their Use for the Treatment of Hepatitis B., 2019.

[16] A. Ciccone, C. Motto, I. Abraha, F. Cozzolino, I. Santilli, Glycoprotein IIb-IIIa inhibitors for acute ischaemic stroke, *Cochrane Database Syst Rev* (3) (2014) CD005208.

[17] T.I. Siddiqui, K.S.A. Kumar, D.K. Dikshit, Platelets and atherothrombosis: causes, targets and treatments for thrombosis, *Curr Med Chem* 20(22) (2013) 2779-97.

[18] J.A. Engelman, Targeting PI3K signalling in cancer: opportunities, challenges and limitations, *Nat Rev Cancer* 9(8) (2009) 550-62.

[19] M. Fiorillo, F. Toth, M. Brindisi, F. Sotgia, M.P. Lisanti, Deferiprone (DFP) Targets Cancer Stem Cell (CSC) Propagation by Inhibiting Mitochondrial Metabolism and Inducing ROS Production, *Cells* 9(6) (2020).

[20] A. Chimento, R. Sirianni, I. Casaburi, C. Ruggiero, M. Maggiolini, S. Ando, V. Pezzi, 17beta-Estradiol activates GPER- and ESR1-dependent pathways inducing apoptosis in GC-2 cells, a mouse spermatocyte-derived cell line, *Mol Cell Endocrinol* 355(1) (2012) 49-59.

[21] E.R. Horak, R. Leek, N. Klenk, S. LeJeune, K. Smith, N. Stuart, M. Greenall, K. Stepniewska, A.L. Harris, Angiogenesis, assessed by platelet/endothelial cell adhesion molecule antibodies, as indicator of node metastases and survival in breast cancer, *Lancet* 340(8828) (1992) 1120-4.

[22] M. Brindisi, M. Fiorillo, L. Frattaruolo, F. Sotgia, M.P. Lisanti, A.R. Cappello, Cholesterol and Mevalonate: Two Metabolites Involved in Breast Cancer Progression and Drug Resistance through the ERRalpha Pathway, *Cells* 9(8) (2020).

[23] S. Mazzotta, L. Frattaruolo, M. Brindisi, C. Ulivieri, F. Vanni, A. Brizzi, G. Carullo, A.R. Cappello, F. Aiello, 3-Amino-alkylated indoles: unexplored green products acting as anti-inflammatory agents, *Future Med Chem* 12(1) (2020) 5-17.

[24] Y. Li, A.R. Cappello, L. Muto, E. Martello, M. Madeo, R. Curcio, P. Lunetti, S. Raho, F. Zaffino, L. Frattaruolo, R. Lappano, R. Malivindi, M. Maggiolini, D. Aiello, C. Piazzolla, L. Capobianco, G. Fiermonte, V. Dolce, Functional characterization of the partially purified Sac1p independent adenine nucleotide transport system (ANTS) from yeast endoplasmic reticulum, *J Biochem* 164(4) (2018) 313-322.

[25] F. Perri, L. Frattaruolo, I. Haworth, M. Brindisi, A. El-magboub, A. Ferrario, C. Gomer, F. Aiello, J.D. Adams, Naturally occurring sesquiterpene lactones and their semi-synthetic derivatives modulate PGE2 levels by decreasing COX2 activity and expression, *Heliyon* 5(3) (2019) e01366.

[26] I. Casaburi, P. Avena, A. De Luca, A. Chimento, R. Sirianni, R. Malivindi, V. Rago, M. Fiorillo, F. Domanico, C. Campana, A.R. Cappello, F. Sotgia, M.P. Lisanti, V. Pezzi, Estrogen related receptor alpha (ERRalpha) a promising target for the therapy of adrenocortical carcinoma (ACC), *Oncotarget* 6(28) (2015) 25135-48.

[27] Y. Samuels, Z. Wang, A. Bardelli, N. Silliman, J. Ptak, S. Szabo, H. Yan, A. Gazdar, S.M. Powell, G.J. Riggins, J.K. Willson, S. Markowitz, K.W. Kinzler, B. Vogelstein, V.E.

- [28] P. Furet, V. Guagnano, R.A. Fairhurst, P. Imbach-Weese, I. Bruce, M. Knapp, C. Fritsch, F. Blasco, J. Blanz, R. Aichholz, J. Hamon, D. Fabbro, G. Caravatti, Discovery of NVP-BYL719 a potent and selective phosphatidylinositol-3 kinase alpha inhibitor selected for clinical evaluation, *Bioorg Med Chem Lett* 23(13) (2013) 3741-8.
- [29] I. Islam, J. Bryant, Y.L. Chou, M.J. Kochanny, W. Lee, G.B. Phillips, H. Yu, M. Adler, M. Whitlow, E. Ho, D. Lentz, M.A. Polokoff, B. Subramanyam, J.M. Wu, D. Zhu, R.I. Feldman, D.O. Arnaiz, Indolinone based phosphoinositide-dependent kinase-1 (PDK1) inhibitors. Part 1: design, synthesis and biological activity, *Bioorg Med Chem Lett* 17(14) (2007) 3814-8.
- [30] G.M. Sastry, M. Adzhigirey, T. Day, R. Annabhimoju, W. Sherman, Protein and ligand preparation: parameters, protocols, and influence on virtual screening enrichments, *J Comput Aided Mol Des* 27(3) (2013) 221-34.
- [31] E. Leung, J.E. Kim, G.W. Rewcastle, G.J. Finlay, B.C. Baguley, Comparison of the effects of the PI3K/mTOR inhibitors NVP-BEZ235 and GSK2126458 on tamoxifen-resistant breast cancer cells, *Cancer Biol Ther* 11(11) (2011) 938-46.
- [32] R.A. Friesner, R.B. Murphy, M.P. Repasky, L.L. Frye, J.R. Greenwood, T.A. Halgren, P.C. Sanschagrin, D.T. Mainz, Extra precision glide: docking and scoring incorporating a model of hydrophobic enclosure for protein-ligand complexes, *J Med Chem* 49(21) (2006) 6177-96.
- [33] J.L. Banks, H.S. Beard, Y. Cao, A.E. Cho, W. Damm, R. Farid, A.K. Felts, T.A. Halgren, D.T. Mainz, J.R. Maple, R. Murphy, D.M. Philipp, M.P. Repasky, L.Y. Zhang, B.J. Berne, R.A. Friesner, E. Gallicchio, R.M. Levy, Integrated Modeling Program, Applied Chemical Theory (IMPACT), *J Comput Chem* 26(16) (2005) 1752-80.
- [34] M. Brindisi, C. Bouzidi, L. Frattaruolo, M.R. Loizzo, M.S. Cappello, A. Dugay, B. Deguin, G. Lauria, A.R. Cappello, R. Tundis, New Insights into the Antioxidant and Anti-Inflammatory Effects of Italian *Salvia officinalis* Leaf and Flower Extracts in Lipopolysaccharide and Tumor-Mediated Inflammation Models, *Antioxidants (Basel)* 10(2) (2021).
- [35] C.D. Bortner, N.B. Oldenburg, J.A. Cidlowski, The role of DNA fragmentation in apoptosis, *Trends Cell Biol* 5(1) (1995) 21-6.
- [36] J. Xi, X. Zhu, Y. Feng, N. Huang, G. Luo, Y. Mao, X. Han, W. Tian, G. Wang, X. Han, R. Luo, Z. Huang, J. An, Development of a novel class of tubulin inhibitors with promising anticancer activities, *Mol Cancer Res* 11(8) (2013) 856-64.
- [37] D. Hanahan, R.A. Weinberg, The hallmarks of cancer, *Cell* 100(1) (2000) 57-70.
- [38] D. Hanahan, R.A. Weinberg, Hallmarks of cancer: the next generation, *Cell* 144(5) (2011) 646-74.
- [39] L. Frattaruolo, M. Brindisi, R. Curcio, F. Marra, V. Dolce, A.R. Cappello, Targeting the Mitochondrial Metabolic Network: A Promising Strategy in Cancer Treatment, *Int J Mol Sci* 21(17) (2020).
- [40] M. Najafi, B. Farhood, K. Mortezaee, Cancer stem cells (CSCs) in cancer progression and therapy, *J Cell Physiol* 234(6) (2019) 8381-8395.
- [41] B.T. Hennessy, D.L. Smith, P.T. Ram, Y. Lu, G.B. Mills, Exploiting the PI3K/AKT pathway for cancer drug discovery, *Nat Rev Drug Discov* 4(12) (2005) 988-1004.
- [42] F. Andre, E. Ciruelos, G. Rubovszky, M. Campone, S. Loibl, H.S. Rugo, H. Iwata, P. Conte, I.A. Mayer, B. Kaufman, T. Yamashita, Y.S. Lu, K. Inoue, M. Takahashi, Z. Papai, A.S. Longin, D. Mills, C. Wilke, S. Hirawat, D. Juric, S.-S. Group, Alpelisib for PIK3CA-Mutated, Hormone Receptor-Positive Advanced Breast Cancer, *N Engl J Med* 380(20) (2019) 1929-1940.
- [43] M.M. Cavalluzzi, G.F. Mangiatordi, O. Nicolotti, G. Lentini, Ligand efficiency metrics in drug discovery: the pros and cons from a practical perspective, *Expert Opin Drug Discov* 12(11) (2017) 1087-1104.
- [44] M.J. Tsai, W.A. Chang, M.S. Huang, P.L. Kuo, Tumor microenvironment: a new treatment target for cancer, *ISRN Biochem* 2014 (2014) 351959.
- [45] L. Bejarano, M.J.C. Jordao, J.A. Joyce, Therapeutic Targeting of the Tumor Microenvironment, *Cancer Discov* 11(4) (2021) 933-959.

Inhibitors and Combination Therapies, *Cancers (Basel)* 13(6) (2021).

[47] H. Pelicano, D.S. Martin, R.H. Xu, P. Huang, Glycolysis inhibition for anticancer treatment, *Oncogene* 25(34) (2006) 4633-46.

[48] S.D. Knight, N.D. Adams, J.L. Burgess, A.M. Chaudhari, M.G. Darcy, C.A. Donatelli, J.I. Luengo, K.A. Newlander, C.A. Parrish, L.H. Ridgers, M.A. Sarpong, S.J. Schmidt, G.S. Van Aller, J.D. Carson, M.A. Diamond, P.A. Elkins, C.M. Gardiner, E. Garver, S.A. Gilbert, R.R. Gontarek, J.R. Jackson, K.L. Kershner, L. Luo, K. Raha, C.S. Sherk, C.M. Sung, D. Sutton, P.J. Tummino, R.J. Wegrzyn, K.R. Auger, D. Dhanak, Discovery of GSK2126458, a Highly Potent Inhibitor of PI3K and the Mammalian Target of Rapamycin, *ACS Med Chem Lett* 1(1) (2010) 39-43.

[49] J. Hao, Y. Zhang, D. Jing, Y. Li, J. Li, Z. Zhao, Role of Hippo signaling in cancer stem cells, *J Cell Physiol* 229(3) (2014) 266-70.

[50] A. Deshmukh, K. Deshpande, F. Arfuso, P. Newsholme, A. Dharmarajan, Cancer stem cell metabolism: a potential target for cancer therapy, *Mol Cancer* 15(1) (2016) 69.

[51] M. Osaki, M. Oshimura, H. Ito, PI3K-Akt pathway: its functions and alterations in human cancer, *Apoptosis* 9(6) (2004) 667-76.

[52] J.A. Fresno Vara, E. Casado, J. de Castro, P. Cejas, C. Belda-Iniesta, M. Gonzalez-Baron, PI3K/Akt signalling pathway and cancer, *Cancer Treat Rev* 30(2) (2004) 193-204.

[53] V. Serra, B. Markman, M. Scaltriti, P.J. Eichhorn, V. Valero, M. Guzman, M.L. Botero, E. Llonch, F. Atzori, S. Di Cosimo, M. Maira, C. Garcia-Echeverria, J.L. Parra, J. Arribas, J. Baselga, NVP-BEZ235, a dual PI3K/mTOR inhibitor, prevents PI3K signaling and inhibits the growth of cancer cells with activating PI3K mutations, *Cancer Res* 68(19) (2008) 8022-30.

[54] S.M. Maira, F. Stauffer, J. Brueggen, P. Furet, C. Schnell, C. Fritsch, S. Brachmann, P. Chene, A. De Pover, K. Schoemaker, D. Fabbro, D. Gabriel, M. Simonen, L. Murphy, P. Finan, W. Sellers, C. Garcia-Echeverria, Identification and characterization of NVP-BEZ235, a new orally available dual phosphatidylinositol 3-kinase/mammalian target of rapamycin inhibitor with potent in vivo antitumor activity, *Mol Cancer Ther* 7(7) (2008) 1851-63.

[55] C. Fritsch, A. Huang, C. Chatenay-Rivauday, C. Schnell, A. Reddy, M. Liu, A. Kauffmann, D. Guthy, D. Erdmann, A. De Pover, P. Furet, H. Gao, S. Ferretti, Y. Wang, J. Trappe, S.M. Brachmann, S.M. Maira, C. Wilson, M. Boehm, C. Garcia-Echeverria, P. Chene, M. Wiesmann, R. Cozens, J. Lehar, R. Schlegel, G. Caravatti, F. Hofmann, W.R. Sellers, Characterization of the novel and specific PI3K $\alpha$  inhibitor NVP-BYL719 and development of the patient stratification strategy for clinical trials, *Mol Cancer Ther* 13(5) (2014) 1117-29.

[56] T. Liu, Q. Sun, Q. Li, H. Yang, Y. Zhang, R. Wang, X. Lin, D. Xiao, Y. Yuan, L. Chen, W. Wang, Dual PI3K/mTOR inhibitors, GSK2126458 and PKI-587, suppress tumor progression and increase radiosensitivity in nasopharyngeal carcinoma, *Mol Cancer Ther* 14(2) (2015) 429-39.

[57] Z. Liu, G. Zhu, R.H. Getzenberg, R.W. Veltri, The Upregulation of PI3K/Akt and MAP Kinase Pathways is Associated with Resistance of Microtubule-Targeting Drugs in Prostate Cancer, *J Cell Biochem* 116(7) (2015) 1341-9.

[58] K. Onishi, M. Higuchi, T. Asakura, N. Masuyama, Y. Gotoh, The PI3K-Akt pathway promotes microtubule stabilization in migrating fibroblasts, *Genes Cells* 12(4) (2007) 535-46.

[59] P. Bhat-Nakshatri, C.P. Goswami, S. Badve, L. Magnani, M. Lupien, H. Nakshatri, Molecular Insights of Pathways Resulting from Two Common PIK3CA Mutations in Breast Cancer, *Cancer Res* 76(13) (2016) 3989-4001.

[60] A. Ruiz-Saenz, C. Dreyer, M.R. Campbell, V. Steri, N. Gulizia, M.M. Moasser, HER2 Amplification in Tumors Activates PI3K/Akt Signaling Independent of HER3, *Cancer Res* 78(13) (2018) 3645-3658.

[61] L.B. Eckert, G.A. Repasky, A.S. Ulku, A. McFall, H. Zhou, C.I. Sartor, C.J. Der, Involvement of Ras activation in human breast cancer cell signaling, invasion, and anoikis, *Cancer Res* 64(13) (2004) 4585-92.

(*rea*).

**Figure 2.** Compounds **2** and **3** exert antiproliferative and cytotoxic effects, inducing apoptotic death in breast cancer cells. Cell viability was assessed in breast cancer cells (MCF-7, MDA-MB-231 and SKBR-3) treated with 100  $\mu$ M of alkyl (*Z*)-2-(2-oxopyrrolidin-3-ylidene)acetates **1-6** (**A**) or using different concentrations (from 25  $\mu$ M to 100  $\mu$ M) of **2** or **3** (**B**). (**C**) MCF-7, MDA-MB-231 and SKBR-3 cells treated at IC<sub>50</sub> values with **2** or **3** for 5 days either without interruption, or else replacing the medium after 24 hours. Cell viability was assessed day by day using SRB. (**D**) Breast cancer cells treated at IC<sub>50</sub> values with **2** or **3** for 5 days were subjected to the comet assay. DAPI was used to stain nuclei. Photographs of slides were taken at 20 $\times$  on a fluorescent microscope, further magnifications of cells were obtained using 100 $\times$  objective. Scale bar 25  $\mu$ m. Values represent mean  $\pm$  SD (n=3) from three independent experiments. \* *P* value < 0.05; \*\* *P* value < 0.01; \*\*\* *P* value < 0.001; \*\*\*\* *P* value < 0.0001.

**Figure 3.** Compounds **2** and **3** induce apoptotic death confirmed by TUNEL assay and decrease proliferation rate of breast cancer cells inhibiting cell cycle. (**A, B, C**) MCF-7, MDA-MB-231 and SKBR-3 cells, respectively, treated at IC<sub>50</sub> values with **2** or **3** for 5 days were subjected to TUNEL assay. DAPI was used to stain nuclei. Photographs of slides were taken at 20 $\times$  on a fluorescent microscope. Scale bar 25  $\mu$ m. (**D**) Histograms represent the % of apoptotic cells vs each control. (**E**) MCF-7, MDA-MB-231 and SKBR-3 cells treated, for 36 hours, with **2** or **3** at IC<sub>50</sub> were subjected to cell cycle analysis. Quantitative analysis of the percentage of cells arrested in different phases of the cell cycle was indicated. Values represent mean  $\pm$  SD (n=3) from three independent experiments. \*\* *P* value < 0.01; \*\*\* *P* value < 0.001; \*\*\*\* *P* value < 0.0001.

**Figure 4.** Compounds **2** and **3** decrease  $\alpha$ -tubulin immunoreactivity in breast cancer cells. Immunofluorescent staining of breast cancer cells (MCF-7 (**A**), MDA-MB-231 (**B**) and SKBR-3 (**C**)) treated with **2** or **3** at IC<sub>50</sub> values for 24 h. DAPI was used to stain nuclei. Pictures were taken at 20  $\times$  magnification. Scale bar 25  $\mu$ m. (**D**) Histograms represent the intensity of fluorescence as results of immunoreactivity of  $\alpha$ -tubulin in

**Figure 5.** Compounds **2** and **3** decrease unlimited division and migratory effects in breast cancer cells. **(A)** Colony-formation assay in breast cancer cells (MCF-7, MDA-MB-231 and SKBR-3) treated with **2** or **3** at  $IC_{50}$  value either for 7 days or else for just one day, replacing the treatment with fresh medium after 24 hours. **(B)** Wound healing scratch assay in MCF-7, MDA-MB-231 and SKBR-3 treated with **2** or **3** at  $IC_{50}$  value for 24 h. Pictures were taken at  $10 \times$  magnification. Scale bars 50  $\mu$ m. Values represent mean  $\pm$  SD (n=3) from three independent experiments. \*\*  $P$  value < 0.01; \*\*\*  $P$  value < 0.001; \*\*\*\*  $P$  value < 0.0001.

**Figure 6.** Compounds **2** and **3** target two cancer features, i.e. new vascular endothelium formation and CSC propagation. **(A)** Tube formation assay in human endothelial cells (Ea HY926) treated, for up to 24 h, with conditioned media (CM) from breast cancer cells treated with **2** or **3** at  $IC_{50}$  value for 24 h. Conditioned media from breast cancer cells treated with vehicle was used as control (CTRL). Pictures were taken at  $20 \times$  magnification. Scale bars 25  $\mu$ m. Red arrows indicate newly formed vessels in the control cells. **(B)** Cell viability of human endothelial cells (Ea HY926) treated for 24 h with conditioned media (CM) from breast cancer cells treated with **2** or **3** at  $IC_{50}$  value for 24 h. Conditioned media from breast cancer cells treated with vehicle was used as control (CTRL). **(C)** Mammosphere formation efficiency assay was performed on breast cancer cells MCF-7, MDA-MB-231 and SKBR-3 after treatment for 5 days with **2** or **3** at  $IC_{50}$  value. Mammospheres were counted using an Olympus BX41 microscope and pictures were taken at  $4 \times$  magnification (with further magnifications at  $10 \times$ ). Scale bars 125  $\mu$ m. Values represent mean  $\pm$  SD (n=3) of three independent experiments. \*\*\*  $P$  value < 0.001.

**Figure 7.** Compounds **2** and **3** act on the PI3K/AKT signaling pathway. **(A)** Immunoblot analysis of the main proteins involved in the PI3K/AKT pathway after treatment with **2** or **3** at  $IC_{50}$  values for 24 h. Optical densities of their expression levels by densitometry are also shown. **(B)** Cell viability assay in breast cancer cells co-treated with **2** or **3** at  $IC_{50}$  values and 20 ng/mL hEGF for 5 days. **(C)** Immunoblot analysis of p-AKT (T308) and p-PI3K p85 after treatment of MCF-7 cells with **2** or **3** at  $IC_{50}$  value for 24 h. Optical densities of their expression levels by densitometry are also shown. **(D)** Immunoblot analysis of PI3K p110 in transfected MCF-7 cells with respect to



MCF-7 cells transfected with empty vector (WT). Optical densities of the different expression levels by densitometry are also shown. **(E)** Viability assay of MCF-7 cells transfected with PCMV-tag ZA PI3KCA-WT (Clone 1) treated with **2** or **3** at its IC<sub>50</sub> for 5 days. Values represent mean ± SD (n=3) from three independent experiments. \* *P* value < 0.05; \*\*\* *P* value < 0.001; \*\*\*\* *P* value < 0.0001.

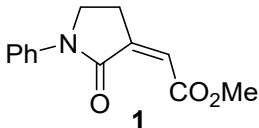
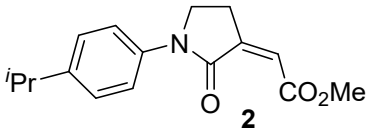
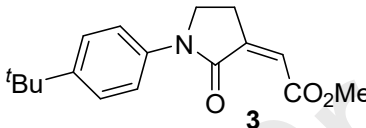
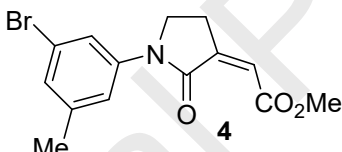
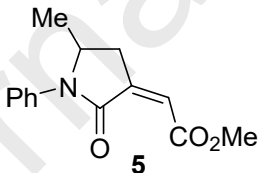
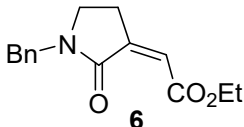
**Figure 8.** Zoomed in view at the PI3K (PDB entry 4JPS) and PDK-1 (PDB entry 2PE0) binding sites in panels (A) and (B), respectively. Top-scored docking poses for **2** and **3** are rendered as green and yellow sticks, respectively while red arrows indicate hydrogen bonds. The cognate ligands, which are alpelisib for PI3K and 39Z for PDK-1, and the functional water molecule are depicted in black and color-type wireframes, respectively.

**Figure 9.** Compounds **8** and **9** interact with plasma proteins and did not exert hemolytic effects. **(A)** Hemolysis assay on RBCs treated with DMSO (CTRL), 0.1% Tween-100, 500µM **2** or 500µM **3** for 1h or 24 h. Histograms represent the relative percentage of hemolysis from three different experiments, each performed with triplicate samples. **(B)** Protein binding assay on plasma protein treated with 500µM **2** or 500µM **3** up to 24 h. Data represent the relative percentage of **2** or **3** bound to the proteins coming from HPLC analysis of three different experiments, each performed with triplicate samples. **(C)** Representative HPLC analysis of free fractions in human plasma of **2** and **3**. Values represent mean ± SD (n=3) of three independent experiments. \*\*\*\**P* value < 0.0001.

### **CRedit authorship contribution statement**

**Matteo Brindisi:** Conceptualization, Investigation, Methodology, Data curation, Writing - original draft, Writing - review & editing. **Luca Frattaruolo:** Conceptualization, Investigation, Methodology, Writing - review & editing. **Raffaella Mancuso:** Conceptualization, Investigation, Writing - review & editing. **Antonio Palumbo Piccionello:** Investigation, Data curation, Writing - review & editing. **Ida Ziccarelli:** Investigation, Writing - review & editing. **Marco Catto:** Investigation, Writing - review & editing. **Orazio Nicolotti:** Investigation, Data curation, Writing - review & editing. **Cosimo Damiano Altomare:** Data curation, Supervision, Writing - original draft, Writing - review & editing. **Bartolo Gabriele:** Conceptualization,

**Table 1.** Structures and lipophilicity of the investigated alkyl (Z)-2-(2-oxopyrrolidin-3-ylidene)acetate derivatives.

Compound	Log <i>P</i> <sup>a</sup>
 <p><b>1</b></p>	0.915
 <p><b>2</b></p>	2.254
 <p><b>3</b></p>	2.603
 <p><b>4</b></p>	2.277
 <p><b>5</b></p>	1.407
 <p><b>6</b></p>	1.483

<sup>a</sup> Calculated by ACDLabs software release 10.0 (Advanced Chemistry Development, Inc., Toronto, Canada).

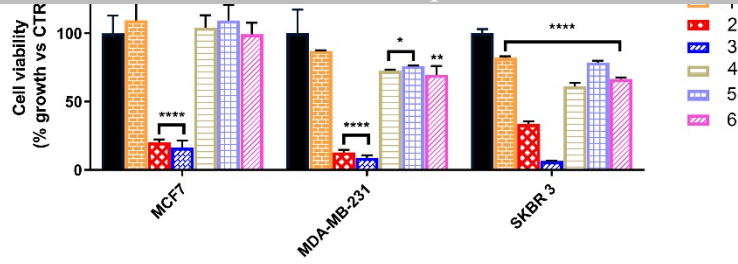
**Table 2.** Cytotoxic activity of  $\gamma$ -lactams **2** and **3**.<sup>a</sup>

Cell Line	<b>2</b>	<b>3</b>	doxorubicin

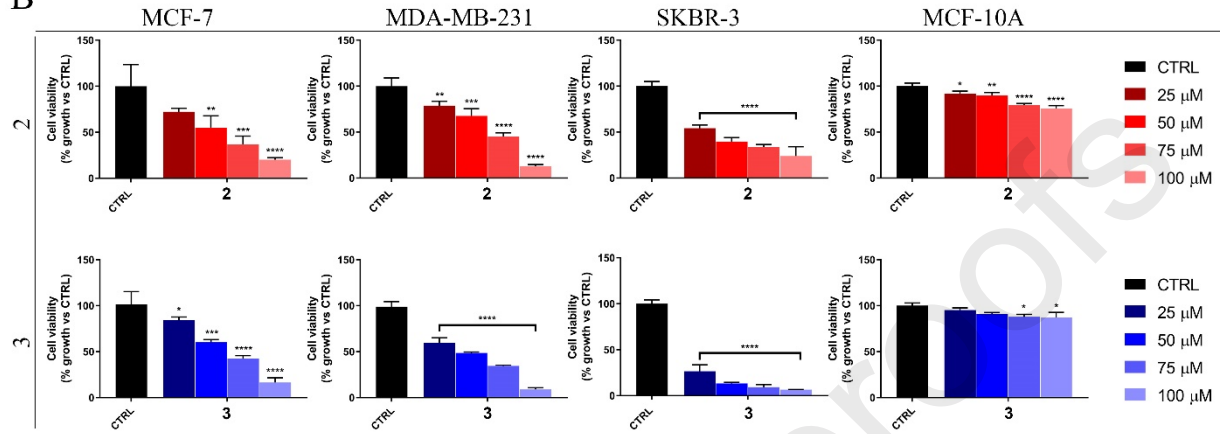
Journal Pre-proofs				
	<b>IC<sub>50</sub> (μM)</b>	<b>47.40</b>	<b>57.26</b>	<b>0.901</b>
	95% confidence interval	35.71 to 62.56	40.01 to 81.96	0.783 to 1.092
	<b>IC<sub>50</sub> (μM)</b>	<b>63.40</b>	<b>34.00</b>	<b>1.213</b>
MDA-MB-231	95% confidence interval	42.56 to 95.30	25.43 to 44.75	0.942 to 1.482
	<b>IC<sub>50</sub> (μM)</b>	<b>32.65</b>	<b>18.34</b>	<b>0.173</b>
SKBR-3	95% confidence interval	27.76 to 38.21	15.94 to 22.73	0.112 to 0.234
	<b>IC<sub>50</sub> (μM)</b>	<b>&gt; 100</b>	<b>&gt; 100</b>	<b>0.354</b>
MCF-10A	95% confidence interval	/	/	0.265 to 0.454

<sup>a</sup> Data are presented as IC<sub>50</sub> values (μM) and 95% confidence intervals obtained by nonlinear regression analysis of three independent experiments.

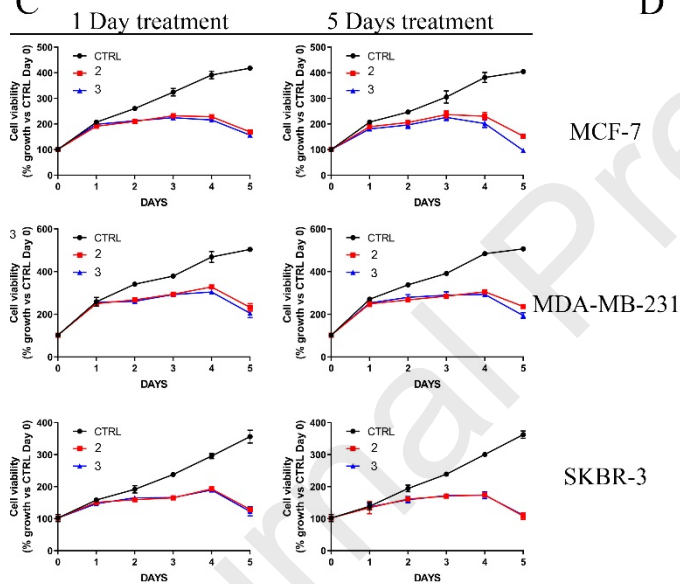
A



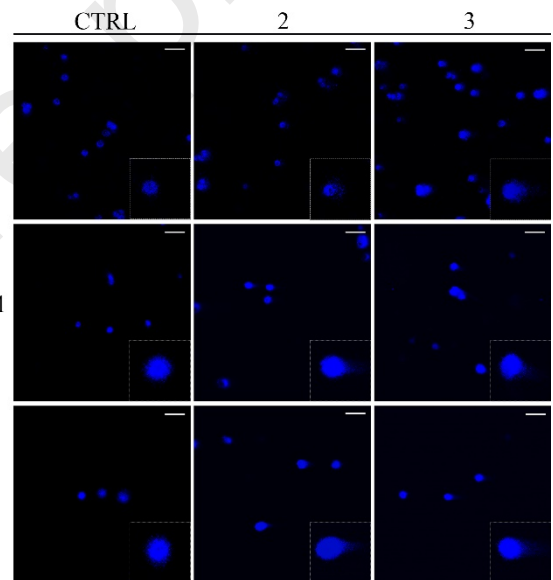
B



C

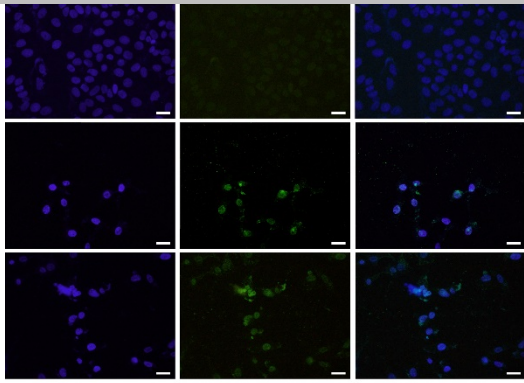


D



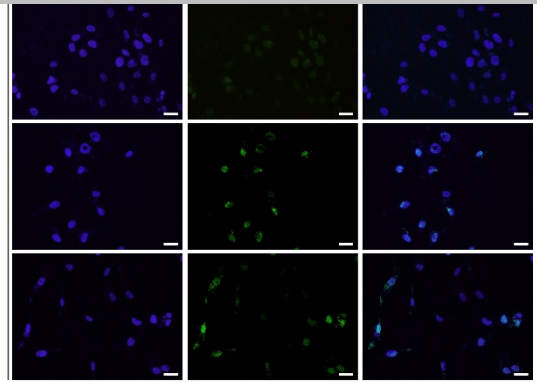
A

MCF-7



B

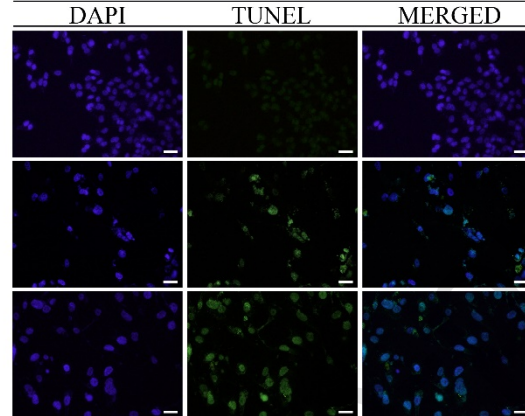
MDA-MB-231



Journal Pre-proofs

C

SKBR-3



CTRL

2

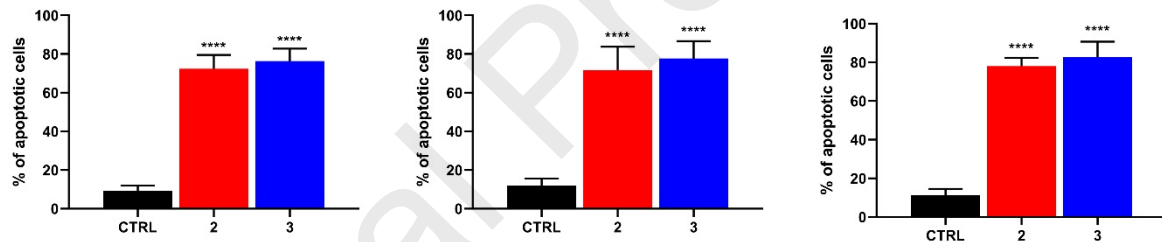
3

D

MCF-7

MDA-MB-231

SKBR-3

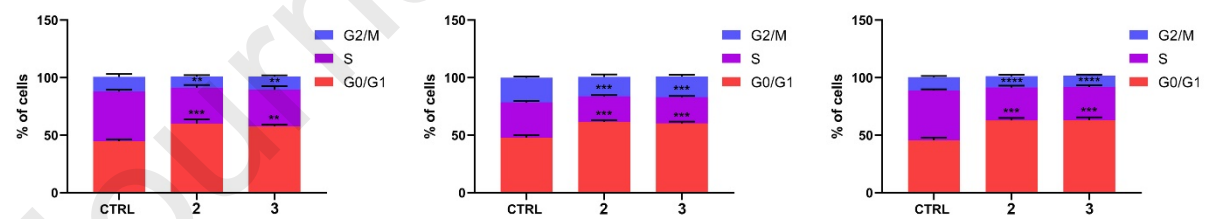


E

MCF-7

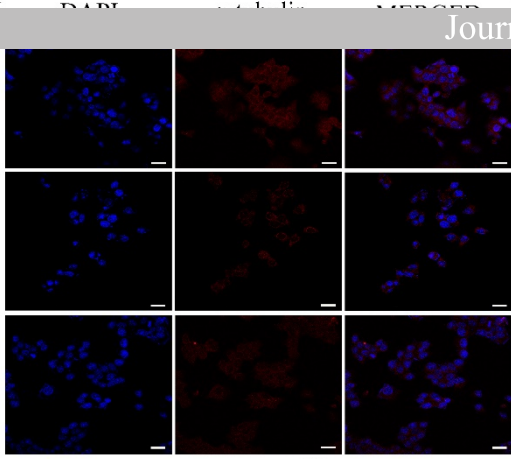
MDA-MB-231

SKBR-3



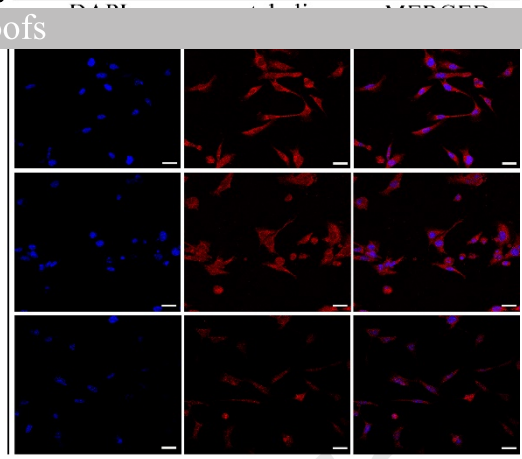
A

MCF-7



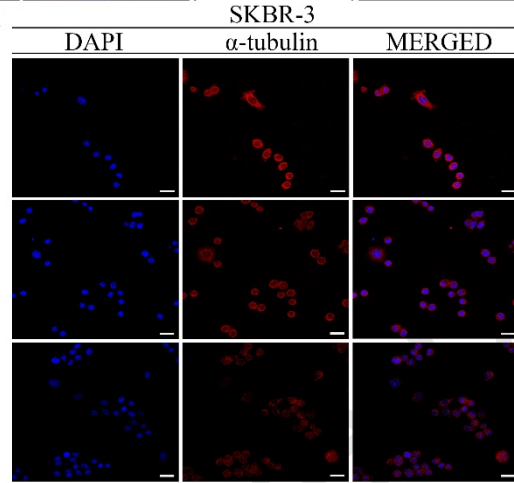
B

MDA-MB-231



Journal Pre-proofs

C

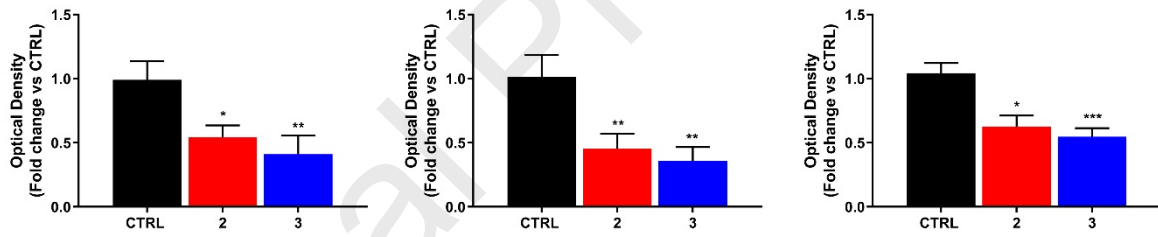


D

MCF-7

MDA-MB-231

SKBR-3



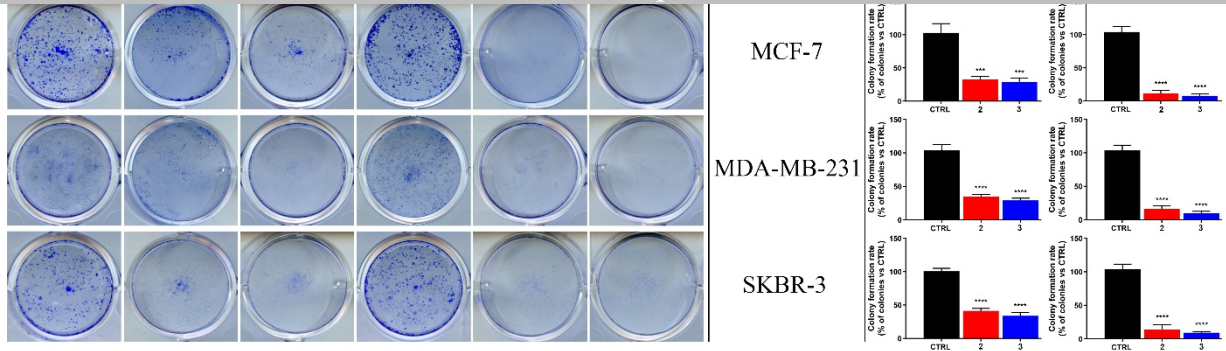
A

1 Day treatment

7 Days treatment

Colony formation rate

Journal Pre-proofs



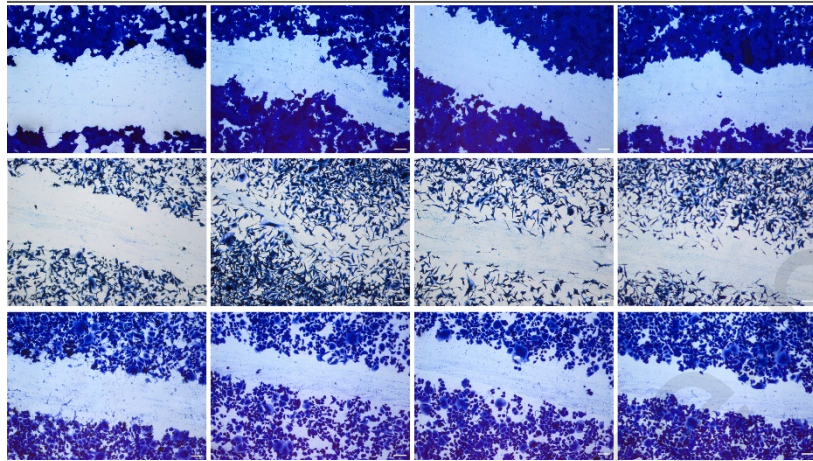
B

CTRL 0 h

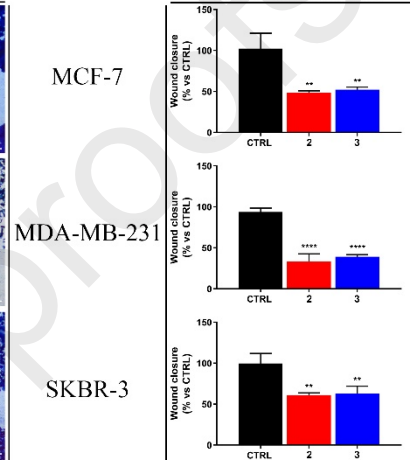
CTRL 24 h

2

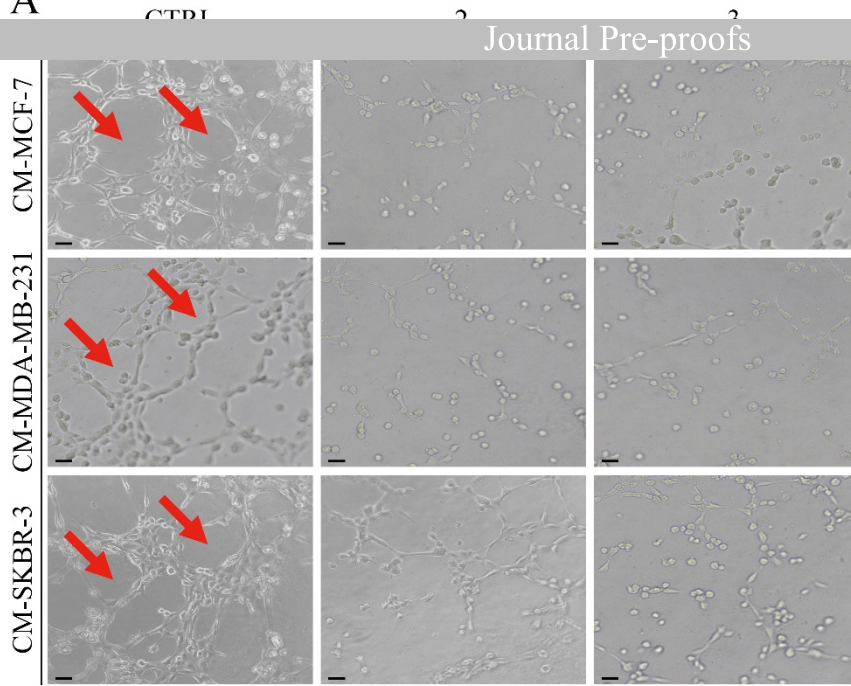
3



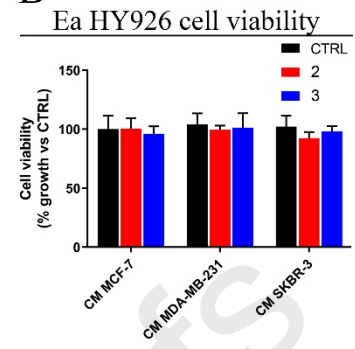
Wound closure rate



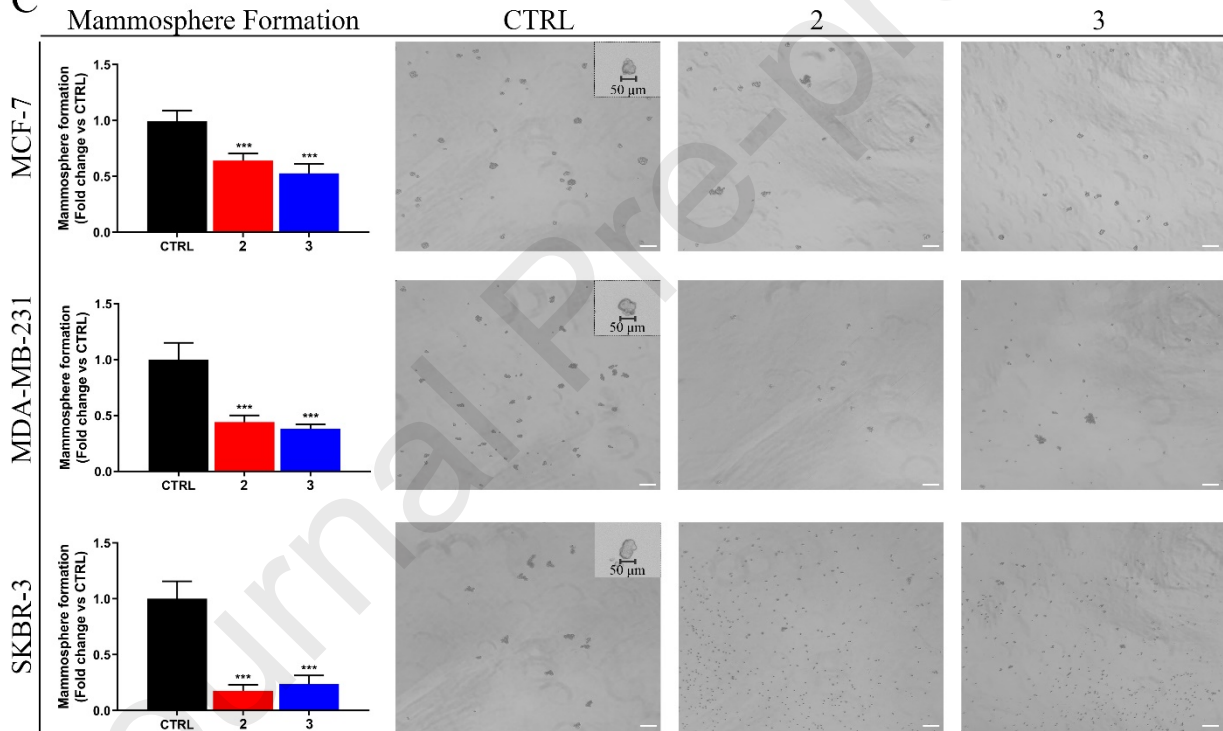
A



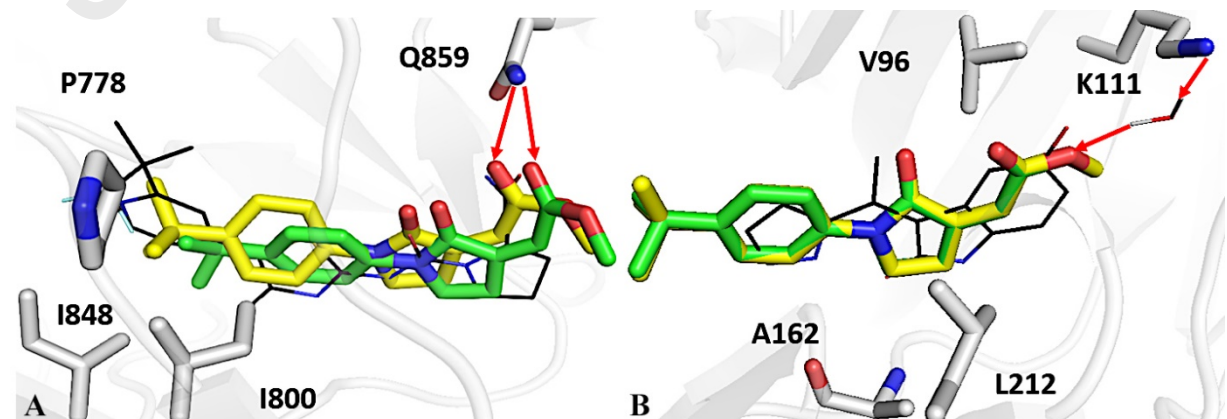
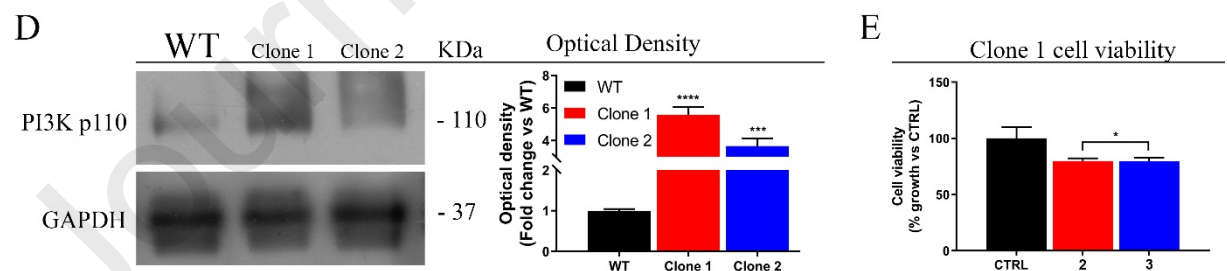
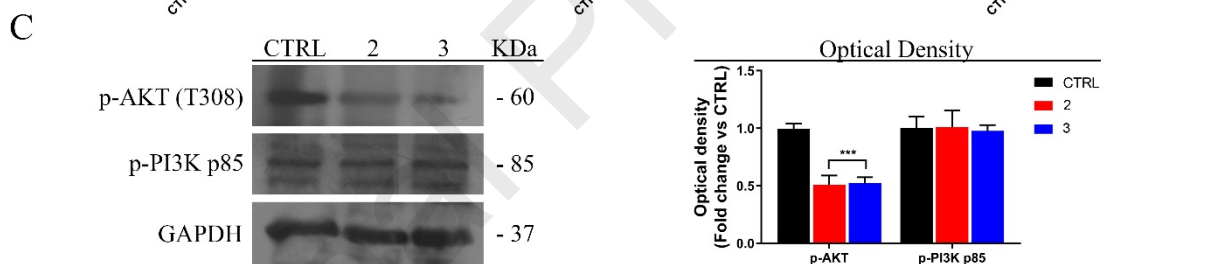
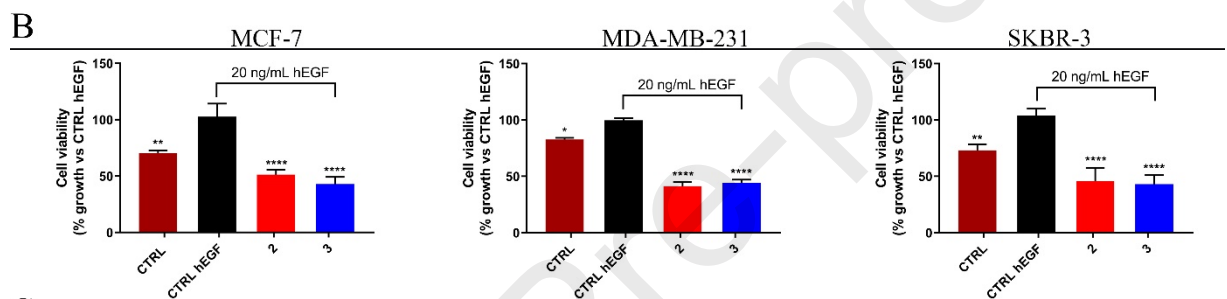
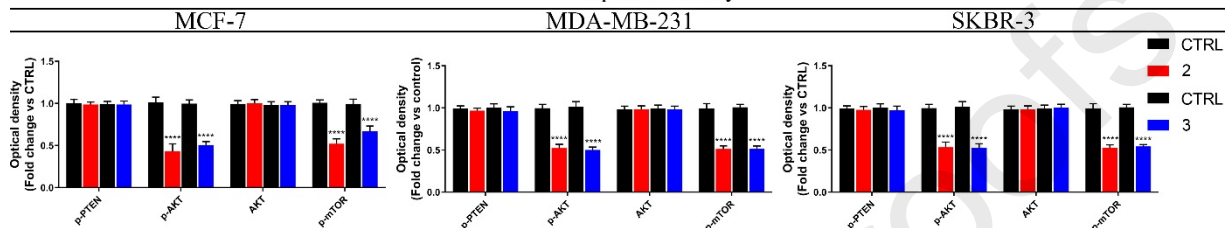
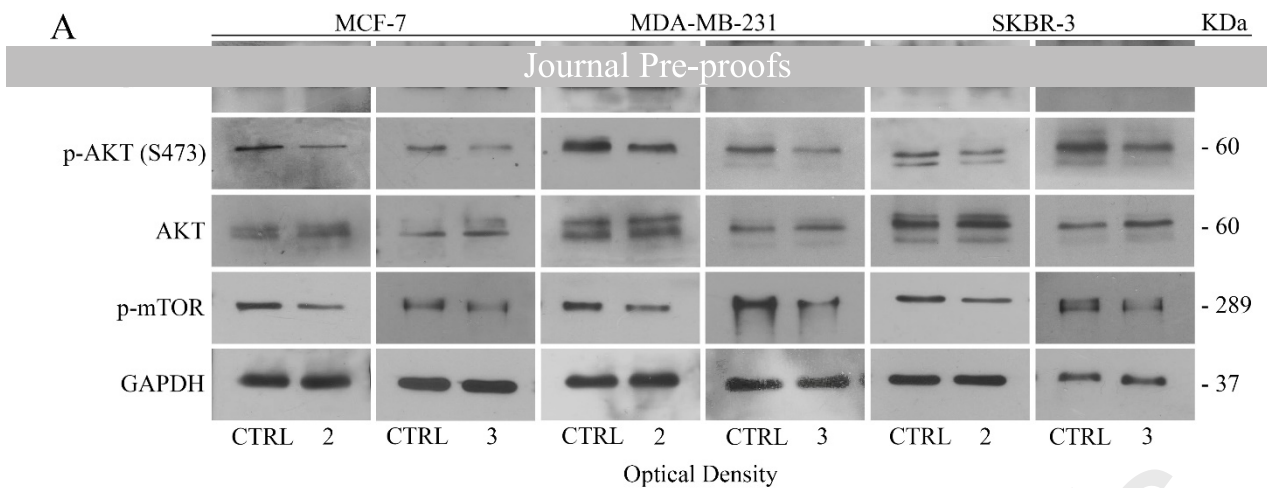
B

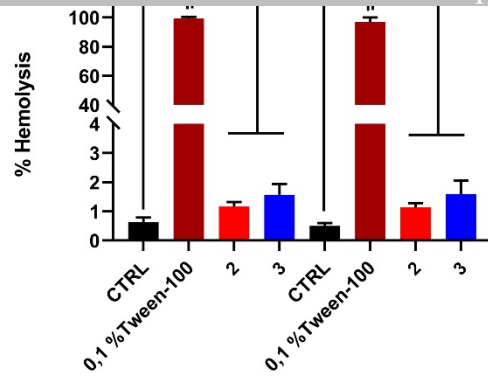


C

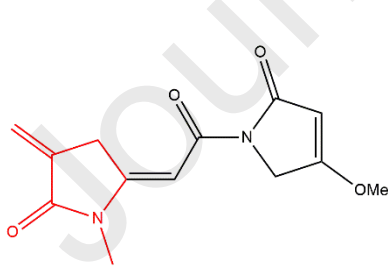
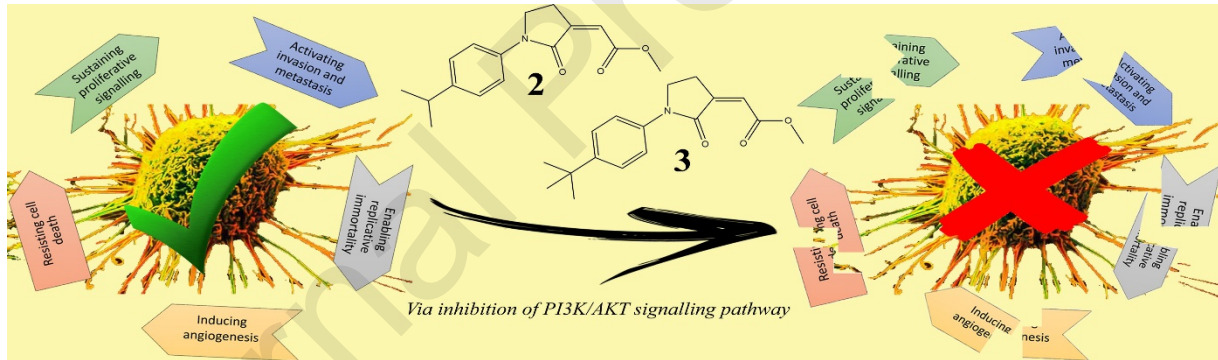
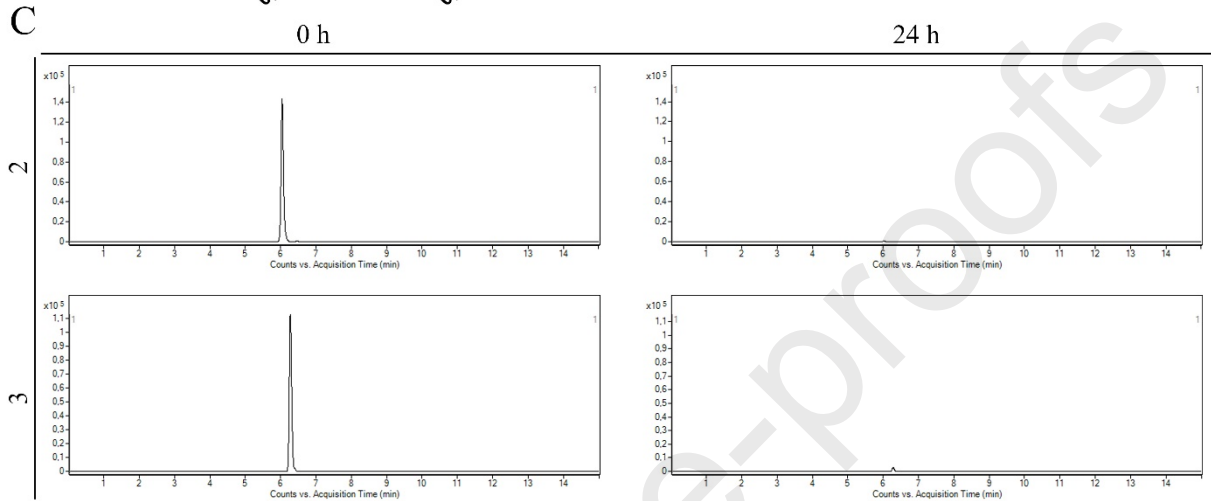




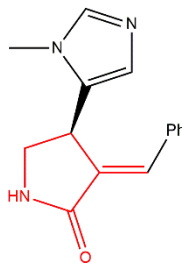




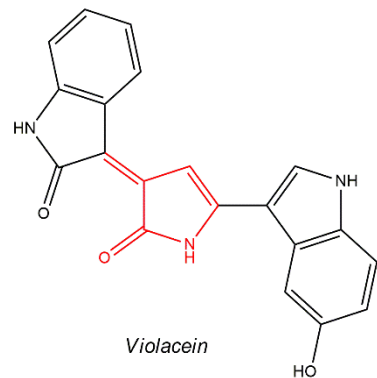
	5 h	24 h
Reboxetine	> 80%	> 90%
2	> 95%	> 95%
3	> 95%	> 95%



Pukeleimide



Anatin



Violacein